Pergamon

PII: S0968-4328(97)00026-7

Micron Vol. 28, No. 3, pp. 197–215, 1997

0968-4328/97 $17.00+0.00

Systematic Investigations of the Contrast Results of Histochemical Stainings of Neurons and Glial Cells in the Human Brain by Means of Image Analysis

OLIVER SCHMITT* and REINHARD EGGERS

Department of Anatomy, Medical University of Lübeck, Ratzeburger Allee 160, D-23538, Lübeck, Germany

(*Received* 8 *July* 1996; *accepted* 20 *March* 1997)

Abstract—The investigation of neurohistological specimens by image analysis has become an important tool in morphological neuroscience. The problems which arise during the processing of these images are non-trivial, especially if a pattern recognition of cells in the imaged tissue is intended. One of the major problems faced concerns the segmentation of structures of interest, whether cells or other histologic structures. The segmentation problem is often the result of an inappropriate staining procedure. For serious image analysis to be performed, the material under investigation must be optimally prepared. Spatially complex patterns, e.g. fuzzy-like neighbouring neurons, are easy to recognize for humans. But the integrative and associative performance of current artificial neuronal network schemes is too low to achieve the same recognition quality as humans do. Therefore, a general analysis of staining characteristics was performed, especially with respect to those stains which are relevant to object segmentation. Although most image analytical investigations of tissues are based on stained samples, a study of this type has not been previously conducted. Of the stains and procedures evaluated, the gallocyanin chrome alum combination staining provided the best stain contrast. Furthermore, this staining method shows sufficient constancy within different parts of the human brain. Even the fine nuclear textures are differentiable and can be used for further pattern recognition procedures. © 1997 Elsevier Science Ltd

Key words: staining, dye, mordant, gallocyanin, neuron, glia, neuropil, CNS, brain, contrast, image analysis, neuroimaging, brain mapping, microdensitometry, colorimetry, videomicroscopy.

INTRODUCTION

Neuroimaging in neuroradiology, brain mapping in positron emission tomography, and functional magnetic resonance tomography are important techniques for basic neuroscience investigations, diagnostics, and therapy (Huerta *et al.*, 1993). The disadvantage of these image methods is a low resolution (Munasinghe *et al.*, 1995); their advantage, however, is the ability to provide noninvasive *in vivo* images. The imaging of post mortem material can be investigated at relatively high spatial resolutions, for example with the help of sensing systems like video cameras attached to optical magnification systems such as light microscopes or confocal laser scanning microscopes. Therewith it is possible to analyse macroscopic or microscopic structures at a level where functional entities or cells can be differentiated. In morphological sciences these projected images of a specimen obtained using a light microscope can be processed by further image analytical methods (light microscopic image analysis, LIA). Generally, the images are converted from analog to digital form. The quality of these images obviously influences their processing. Therefore, it is necessary to optimize the analog material and the converter itself. Most problems at the analytical level of image processing are caused by problems of preprocessing, and in morphology it is the differentiation caused by any histological staining of the analog material. The differentiation or histological difference is considered here as the distance between the foreground (structures of interest or SOI) and the background of a certain stained tissue. The differentiation of structures in paraffin sections can be done with many different histological methods. Because histochemical staining procedures are commonly used in neurohistology, these methods were taken into consideration. Other disciplines which make use of image analysis techniques are concerned with the problems described above (Camby *et al.*, 1995; Decaesteck *et al.*, 1995), which shows the general importance of these investigations.

High resolution (Toga and Arnica-Sulze, 1987; Toga, 1990; Toga and Banerjee, 1993; Toga *et al.*, 1994; Toga, 1995) has been applied in the analysis of macroscopic neurological structures. In light microscopy, a

*Corresponding author: e-mail: schmitt@anat.mu-luebeck.de

Abbreviations: ap, acetate buffer; C, contrast; CCD, charge-coupled device; C.I., color index; CIE-XYZ, Commision Internationale de l'Éclairage, X, Y and Z are the primary colors of the CIE color diagram; CMY, cyan, magenta, yellow color model; CNS, central nervous system; DNA, desoxyribonucleic acid; DIN, Deutsche Industrie Norm (German industry normalisation commitee); EHC, enzymehistochemical; g, glial cell; HR, high resolution; HSI, hue, saturation, intensity value color model; i, Neuropil; I, intensity; IHC, immunohistochemical; IOD, integrated optical density; LIA, light microscopic image analysis; LUT, look up table; lux, intensity of luminance; m, meth, method; MHR, magnified high resolution; MOD, mean optical density; MUR, magnified ultrahigh resolution; n, neuron; NA, numerical aperture; O, optimum value; PAD, piezo-controlled aperture displacement; r, number of pixels in an image region (size of region in pixels); RGB, additive red, green, blue color model; ROI, region of interest; RT, room temperature; SMM, spatial multiplex method; SOI, structure of interest; vero, veronal acetate buffer; YIQ, luminance (=primary color Y of the CIE model), I color code, Q color code; zpp, citric acid disodium phosphate buffer; zzp, citric acid sodium citrate buffer.

differentiation between high resolution (HR) video techniques ($\leq 1024 \times 1024$ pixel), magnified high resolution (MHR) video techniques (Amunts *et al.*, 1995; Eins, 1974; Eins and Wilhelms, 1976; Eins and Gallyas, 1977, 1978; Forbes and Petry, 1979; Sauer, 1980, 1983a, 1983b, 1983c; Sauer *et al.*, 1986; Schleicher *et al.*, 1986; Schleicher, 1990; Wree *et al.*, 1982, 1983a, 1983b; Zilles, 1978a, 1978b; Zilles *et al.*, 1979a, 1979b, 1980; Zilles, 1981; Zilles *et al.*, 1983, 1984, 1986) and magnified ultrahigh resolution (MUR) video techniques ($>1024 \times 1024$ pixel), as is used here, can be made. MHR and MUR LIA are important quantitative tools of morphoquantitative analysis because high resolution information of cell features can be obtained. The increase of image information has the advantage that subsequent classification tasks can be performed more reliably than with images obtained through low resolution sources.

Generally, the motivation for MUR LIA is to get a more objective analysis of any part of the nervous system at the cellular level independent of human intervention. The results are quantitative relations between different neuronal populations or other entities during their development, in disease and in maturity. Furthermore, their properties of spatial geometrics or spatial distribution can be detected by point pattern analysis (Schmitt *et al.*, 1995b).

In the past, automatic as well as semiautomatic image analysis of the brain was performed with stains such as cresyl violet (Sauer *et al.*, 1986), Gallyas' silver method (Eins and Gallyas, 1977; Gallyas, 1993) and methylene blue (Berkowitz *et al.*, 1968; Lindroos, 1991; Müller, 1994; Perry, 1981) which seemed to be optimal. However, by means of these dyes the segmentation of structures of interest (SOI) as neurons, glia cells, endothelial cells and ependymal cells is difficult. The reason for this difficulty is the relatively intense staining of the neuropil and too low a staining of the SOIs (Ahrens *et al.*, 1990; Amunts *et al.*, 1995; Istomin and Amunts, 1992). Furthermore, the overlapping of optical section planes reduces the contrast of SOIs and background. Therefore, many investigations of HR LIA are performed using gray value statistics or the gray-level index method as introduced by Schleicher *et al.* (1978), Schleicher and Zilles (1983) (Amunts *et al.*, 1995; Eins and Gallyas, 1977; Sauer *et al.*, 1986; Wree *et al.*, 1982; Zilles, 1978a) and less often by methods of pattern recognition where SOIs are classified.

In order to compare different staining results, it is necessary to quantify contrast. High contrast staining requires a maximal staining of SOIs but a minimal staining of the neuropil, for example black SOIs and opaque neuropil. On the other hand, such staining is not optimal because fine structures of the SOIs cannot be recognized (Eins and Gallyas, 1977; Herlin *et al.*, 1989). If the fine structures (nucleus and nucleolus borders) of neurons are masked by overstaining it is not possible to classify neurons into different populations by their morphological features.

This SOI-orientated contrast definition must be distinguished from the general contrast definition (Levine, 1985), with intensities which can be extended to the spatial modulation transfer function which is equivalent to the inverse of the threshold of contrast perception (contrast sensitivity function) (Levine, 1985).

A further problem arises from the different staining properties of different regions of the human brain (Haug, 1976). For example, using the stain cresyl violet, the glia cells of the hippocampus are stained less than those in the neostriatum, and the cytoplasm of neurons in the fascia dentata are stained less than those in CA4 of the hippocampus.

The decision to use histochemical staining procedures and not immunohistochemical (IHC) or enzymehistochemical (EHC) ones was made considering the efficiency of the methods with respect to large mapping tasks. The optimal method should be useable on *large serial* sections up to $200 \times 200\ mm^2$ as well as on small ones. Application of an IHC method would give efficient morphological and specific staining results but high costs when large serial sections have to be stained (Agnati *et al.*, 1986; Holmbom *et al.*, 1991). EHC is not efficient because large specimens will contain too many artifacts caused by crystallization in frozen materials (Heinsen and Heinsen, 1991; Hine and Rodriguez, 1992; Holmbom *et al.*, 1991; Rosene *et al.*, 1986). Fluorescence stains were not investigated because, even after the addition of anti-bleaching or anti-fading substances (Berios, 1995; Giloh, 1982; Kriete, 1992; Mason *et al.*, 1993; Talve *et al.*, 1995), the rate of specimen bleaching is too fast and would cause an extreme signal loss within automatic MUR LIA.

The seven most important criteria for the characterization of an optimal staining protocol for automatic MUR LIA are: (1) contrast and selectivity (maximal affinity of a dye to SOIs and a minimal affinity to the neuropil); (2) differentiation (capability to differentiate the intracellular structures of SOIs); (3) similarity or constancy (homogeneous contrast of SOIs in different brain regions); (4) standardization (minimum number of differentiation steps within the staining procedure); (5) efficiency and simplicity (low material and personal costs of the staining procedure); (6) stability (staining quality and contrast should not change); and (7) clearness (no artifacts caused by crystallization or agglomeration of chelate complexes).

Unfortunately there are no publications adressing systematic measurements of staining results of paraffin sections by colorimetric or microdensitometric methods. A survey of neuronal stainings with documented histological images in color was published by Heimann (1898). Since then, there has been nothing else published that is comparable. However, there exists an enormous amount of data on the special stainings of SOIs in the CNS, of which only a selection is cited (Böck, 1979; Braak, 1984, 1988; Clark and Clark, 1971; Clark, 1973; Duckett and Triggs, 1965; Eggers, 1990; Eichler and Taylor, 1976; Eins and Gallyas, 1977; Eins, 1973; Fischer *et al.*, 1961; Gabe, 1976; Gallyas, 1993; Heinsen and Heinsen, 1991; Herlin *et al.*, 1989; Howard, 1979; Oud *et al.*, 1981; Powers, 1960; Rális *et al.*, 1973;

Reusche, 1991; Romeis, 1989; Schmitt *et al.*, 1995a; Segarra, 1970; Supprian *et al.*, 1993; Tolivia *et al.*, 1994; Vacca, 1985; Wenzelides, 1982).

In order to obtain optimal MUR LIA results, it is important to know and apply the optimal staining protocol for the analysis of SOIs by a sophisticated MUR LIA system. (Camby *et al.*, 1995; Decaesteck *et al.*, 1995).

The goal of this study is to find an optimal staining procedure for MUR LIA, similiar to what has been done with Feulgen staining (Thiessen and Thiessen, 1977) and its modifications by Camby *et al.*, (1995) and Decaesteck *et al.* (1995) for DNA and nuclei image analysis. Therefore, an extensive investigation of the contrast properties of more than 80 staining protocols was performed.

MATERIALS AND METHODS

Six normal adult human brains were perfused through peripheral arteries with a 4% phosphate buffered (pH 7.4) formalin solution. These brains were sectioned into small blocks of $20 \times 20 \times 10\ mm^3$ and kept between 4 and 12 weeks in a buffered formalin bath at 4°C. This immersion step was followed by rinsing of the specimens in tapwater for 12 h. Embedding in 1 portion paraffin wax and intermedium (1p+1p) and 2 portions paraffin wax (Paraplast®) at 60°C was done following the intermedia absolute ethanol or methylbenzoate. However, the choice of intermedia (ethanol, isopropyl alcohol, methylbenzoate) does not change the staining results significantly. Also, the choice of embedding media results in no significant differences following cresyl violet staining (Haug and Kraus, 1958), and was not investigated here.

All paraffin blocks were sectioned into 12 μm thick slices which were stretched in a 56°C water bath and mounted on slides covered by a cellulose filtered protein glycerol (1p+1p) solution. After drying at 37°C for 3 days, the sections were deparaffined in 5 portions xylene and rehydrated in a graded series from absolute down to 70% ethanol and then put into demineralized water.

In the first step of the experiment, staining procedures were performed according to the standard methods of Gabe (1976), Rális *et al.* (1973), Romeis (1989) and Vacca (1985) and of recently developed neurohistological staining techniques. This first step was performed to help in selecting staining procedures that provide intensive contrast characteristics for further investigations. A complete list of all stains and their references is given in Table 1. The dyes used are all characterized chemically in The Colour Index (1971), Harms (1965), Clark (1973), Gray (1975), Gabe (1976), Green (1991) and Schmidt and Merck (1993). Mainly nuclear stainings and stainings of the neuronal perikarya were tested. Some silver stainings were performed, too. Silver impregnations were not investigated because, according to the stain mode of action, not all neurons were impregnated and therefore impregnation results were irregular (Spacek, 1992).

Any differentiation after the staining was avoided in order to obtain standardized and comparable results. However, optimal dehydration times were defined for each stain.

After staining, the sections were dehydrated in graded ethanol from 70% to 100% and then through 5 portions of xylene. They were then mounted in Entellan®.

If a staining procedure produced high contrast within SOIs, the staining procedure was further examined in a second step experimenting with buffering, dye concentrations and incubation temperature in order to optimize it.

We investigated the influence of 4 buffer systems on aqueous solutions of different stains. Acetate buffer, veronal acetate buffer or Michaelis buffer, citrate acid phosphate buffer and citrate acid citrate buffer were used because their buffering ranges from 3.8 to 4.2. On this small pH range the staining results of SOIs showed the largest changes. If the staining solution was alcoholic, the dye concentration was varied. Finally, the incubation temperature was varied between room temperature and 37°C.

The sections were analysed with the IBAS® image analysis system from KONTRON®. The programmable high resolution piezo-controlled aperture displacement (PAD) RGB solid state sensing charge coupled device (CCD camera) ProgRes® 3012 (2996 horizontal $\times$ 3060 vertical pixels; 12 bit resolution in each color channel) was used for microdensitometric measurements (Goldstein, 1980; Lewis, 1991). Color information was obtained by the spatial multiplex method (SMM), using a mosaic color filter on the sensor. Therefore, no further filters in the microscope were used, as described by Rüter *et al.* (1978, 1979, 1980). The advantage of this method is stable color convergence. The filter variation over time through PAD and by geometry through the SMM is based on the Dresler-principle (DIN 5033, 1993). The relative spectral response to the RGB signals lies between 0.6 for red and 1.0 for green with spectral peaks for blue, green and red at roughly 450 nm, 530 nm and 580 nm. The relative spectral response of the camera fulfils the condition of Luther for calibration and sensitivity of color filters (DIN 5033, 1993).

The disadvantage of the SMM is a reduction of resolution which is compensated by using microscanning with PAD. The color Moiré effect and other color convergence errors are eliminated because at each sampling site all color channels receive the same image information (co-site sampling). At least three monochromatic images consisting of the three primary colors red, green and blue, according to the trichromatic color theory (Gonzalez and Woods, 1993), were received. The three monochromatic images can be composed into one multispectral (Sonka *et al.*, 1993) image. Therefore, the analysis was performed in a three-dimensional color space or multidimensional color space, also called a

Table 1. Used staining procedures and their dye characteristics (Clark, 1973; Gabe, 1976; Gray, 1975; Harms, 1965; Schmidt and Merck, 1993)

Dye		C.I.	CAS	Dye class	Staining character	Staining method
AgNOR cresyl violet			10510-54-0	Oxazin	basic	Reusche, 1991
Alcian blue 8GX pH 2.5/(4.0 30 min)		74240	75881-23-1	Phthalocyanin	basic	Vacca, 1985
Aldehyde fuchsin cresyl violet		42500	569-61-9	Phthalocyanin	basic	Schmitt *et al.*, 1995a
cresyl violet			10510-54-0	Phenyl methane	basic	
Alizarin blue black B		63615	1324-21-6	Anthrachinon	acid	Vacca, 1985
Alizarin blue S		67415	130-22-3	Anthrachinon	acid	Vacca, 1985
Alphazurine A		42080	3486-30-4	Phenyl methane	acid	Schmitt, 1995c
Aniline Schiff	Aniline blue	42775	8004-91-9	Phenyl methane	basic	Romeis, 1989
	Pararosaniline	42500	569-61-9	Phenyl methane	basic	
Aniline blue		42775	8004-91-9	Phenyl methane	basic	Romeis, 1989
Aniline black		50440	13007-86-8	Azine	acid	Wenzelides, 1982
Azan	Azocarmine B	50090	25360-72-9	Azine	basic	Romeis, 1989
	Anilin blue	42775	8004-91-9	Phenyl methane	basic	
Azure A		52005	531-53-3	Thiazin	basic	Vacca, 1985
Azure A phenol		52005	531-53-3	Thiazin	basic	Vacca, 1985
Azure B pH 4.2		52010	531-55-5	Thiazin	basic	Vacca, 1985
Azure B phenol		52010	531-55-5	Thiazin	basic	Vacca, 1985
Azure C pH 4.2		52002	531-57-7	Thiazin	basic	Vacca, 1985
Bielschowsky Plien cresyl violet			10510-54-0	Oxazin	basic	Rális *et al.*, 1973
Bismarck brown Y		21000	10114-58-6	Poly-azo	basic	Vacca, 1985
Brazilin		75280	474-07-7	Natural	acid	Romeis, 1989
Brillant cresyl blue		51010	81029-05-2	Oxazine	basic	Romeis, 1989
Brillant cresyl blue 2h		51010	81029-05-2	Oxazine	basic	Romeis, 1989
Brillant black		28440	2519-30-4	Di-azo	basic	Schmitt, 1995c
Brillant black without KBr		28440	2519-30-4	Di-azo	basic	Schmitt, 1995c
Chrome alum	hemalum		7788-99-0			Vacca, 1985
	hemalaun	75290	517-28-2	Natural	acid	
Chrome alum	carmine		7788-99-0	Anorganic		Vacca, 1985
	carmine	75470	1390-65-4	Natural	acid	
Celestine blue B		51050	1562-90-9	Oxazine	basic	Vacca, 1985
Celestine blue B without Fe		51050	1562-90-9	Oxazine	basic	Vacca, 1985
Darrow red method I			15391-59-0		basic	Braak, 1988
Darrow red method II			15391-59-0		basic	Schmitt, 1995c
Formol thionin		52000	78338-22-4	Thiazin	basic	Tolivia *et al.*, 1994
Gallocyanin	chrome alum GBL2	51030	1562-85-2	Oxazine	basic	Vacca, 1985
	chrome alum		7788-99-0	Anorganic		
Gallocyanin	chrome alum meth2	51030	1562-85-2	Oxazine	basic	Vacca, 1985
	chrome alum		7788-99-0			
Gallyas				Silver		Gallyas, 1993
Gordon Sweet reticulin				Silver		Rális *et al.*, 1973
Hemalum (hematoxylin)	eosin	75290	517-28-2	Natural	acid	Vacca, 1985
	eosin	45380	17372-87-1	Xanthene	acid	
Heidenhain iron hemalum O GBL1		75290	517-28-2	Natural	acid	Vacca, 1985
hemalum (hematoxylin)		75290	517-28-2	Natural	acid	
Heidenhain iron hemalum		75290	517-28-2	Natural	acid	Vacca, 1985
Helds molybdenum hemalum		75290	517-28-2	Natural	acid	Rális *et al.*, 1973
Howard + hemalum eosin		75290	517-28-2	Silver		Howard, 1979
hemalum (hematoxylin)		7529	517-28-2	Natural	acid	
	eosin	45380	17372-87-1	Xanthene	acid	
Iron alizarin blue black B		63615	1324-21-6	Anthraquinone	acid	Vacca, 1985
Nuclear fast red		60760	6409-77-4	Anthraquinone	acid	Vacca, 1985
Kluever Barrera:	luxol fast blue MBSN	74180	1328-51-4	Phthalocyanin	basic	Romeis, 1989
Korson + hemalum eosin				Silver		Korson, 1964
hemalum (hematoxylin)		75290	517-28-2	Natural	acid	
	eosin	45380	17372-87-1	Xanthene	acid	
Cresyl violet			10510-54-0	Oxazine	basic	Vacca, 1985
Cresyl violet + KBr			10510-54-0	Oxazine	basic	Vacca, 1985
Cresyl violet method 3 pH 4.0			10510-54-0	Oxazine	basic	Vacca, 1985
Masson Goldner						Romeis, 1989
Ponceau S		27190	6226-78-4	Poly-azo	acid	
Anilin blue		42775	8004-91-9	Phenyl methane	basic	
Weigerts iron hematoxylin		75290	517-28-2	Natural	acid	
Methylene blue		52015	7220-79-3	Thiazin	basic	Vacca, 1985
Methylene blue	basic fuchsin	52015	7220-79-3	Thiazin	basic	Romeis, 1989
	basic fuchsin	42500	569-61-9	Phenyl methane	basic	
Methylene blue Schabadasch		52015	7220-79-3	Thiazin	basic	Romeis, 1989
Methylene blue polychrome		52015	7220-79-3	Thiazin	basic	Romeis, 1989
Methyl green	pyronin Y	42585	7114-03-6	Triarylmethane	basic	Vacca, 1985
	pyronin Y	45005	92-32-0	Xanthene	basic	
New fuchsine		42520	3248-91-7	Phenyl methane	acid	Romeis, 1989
New methylene blue N		52030	6586-05-6	Thiazin	basic	Vacca, 1985
Nile blue sulfate		51180	3625-57-8	Oxazine	basic	Vacca, 1985
Parafuchsin base		42500	569-61-9	Phenyl methane	basic	Braak, 1984
Patent blue violet		42045	129-17-9	Phenyl methane	acid	Schmitt, 1995c
Pischingers methylene blue		52015	7220-79-3	Thiazin	basic	Gabe, 1976
Pyrrole blue B*				Isantine	basic	Schmitt, 1995c
Richardson	Methylene blue	52015	7220-79-3	Thiazin	basic	Romeis, 1989
	Azure B	52010	531-55-5	Thiazin	basic	

Table 1—continued

Table 1—*continued*

Dye	C.I.	CAS	Dye class	Staining character	Staining method
Safranine O method I-IV	50240	477-73-6	Azin	basic	Romeis, 1989
Sudan black B	26150	4197-25-5	Poly-azo	lysochrome	Vacca, 1985
Thiazine brown R	20220		Thiazin	basic	Schmitt, 1995c
Thionine	52000	78338-22-4	Thiazin	basic	Schmitt, 1995c
Toluidine blue	52040	92-31-9	Thiazin	basic	Vacca, 1985

* Pyrrole blue is the reaction product of isatine with pyrrol after Deutsche Chemische Gesellschaft (1935), Deutsche Chemische Gesellschaft (1953) and Harms (1965).

trivariance space (Levine, 1985). In the following, the term colorimetry is used for the measurements of the transmission τ_i (transmission factor) of a certain range of light waves ($\lambda_{R,G,B}$) through the absorbing section (absorption volume) by the CCD camera, where Φ is the light intensity.

$$\tau_i(\lambda_{R,G,B})=\frac{\Phi_{outcoming}(\lambda_{R,G,B})}{\Phi_{incoming}(\lambda_{R,G,B})}.$$

This method of measuring color is also called the tristimulus method of colorimetry because the three primary colors are analyzed.

Brightness or optical density of SOIs in each color channel is measured by an interactive image analytical procedure after analog-to-digital conversion by the CCD camera (Sonka *et al.*, 1993), but not by photometry since the objects are not light sources (Klein-Wisenberg, 1981; Piller, 1977; Pratt, 1978). After a comparison of different resolutions, a programmable resolution of 2994 (horizontal, 2.83 μm) × 1740 (vertical, 3.67 μm) active pixels at an optical magnification of 1250 times was selected for the colorimetric measurements. The maximal and minimal sensitivities of the camera using F=5.6 are, respectively, 10000 lux and 40 lux, and 312 lux and 1.25 lux using F=1.0. The dynamic range (Capowski, 1989) of this camera is smaller than that of most monochromatic cameras. However, this relatively low sensitivity is compensated by signal enhancement by using the gain function. A final object magnification of 2560× at the display device was attained with a resolution of 0.13 μm edge length per pixel. Taking these parameters into account, one image consists of 144 micro-scanned partial images requiring 22 MB storage space. It takes 11.52 s for data transfer and calculation of the final color image. The camera is attached to the 'Großes Universalforschungsmikroskop' from Zeiss, which is installed on a vibration-damped table in order to reduce vibration effects during image generation. All measurements were performed with a ×100 oil immersion planapochromatic objective (NA 1.25) in combination with a 1.25× auxiliary lens. In order to avoid nonlinearities due to the modulation transfer function, a high optical magnification and small objective aperture was chosen (Ramm and Kulick, 1985). The illumination is based on the Köhler illumination technique (Romeis, 1989). The light source is a 24 V, 100 W halogen lamp which produces a diffuse achromatic light of a temperature of about 3200 K (2100 cd/cm^2) which is stabilized by a light control unit.

Each color channel with a digitization depth of 12 bits or 4096 values was scaled to an 8 bit gray level image with 256 densitometric or intensity levels before beginning the measurements. The determined contrast is based on a comparison between SOI and neuropil. Therefore, red (R), green (G) and blue (B) chromaticity values (the definition of the functions of spectral power distributions of the CIE primary colors can be found in Foley *et al.*, 1994) of neurons (n), glia cells (g) and neuropil (i) were measured. The final contrast is the mean contrast of all color channels. The calculation and comparison of contrasts were performed within the additive RGB system. Transformations from RGB into HSI, CIE-DIN (normal color valence system), YIQ or CMY color space (Foley *et al.*, 1994) were not applied because an adaption to human color vision for subjective contrast evaluations was not necessary (Albert *et al.*, 1993). Color changes which can be seen better in HSI images (Russ, 1991) were of minor interest because the quantification of intensities in the single color channels allows one to detect higher contrast than in transformed HSI images. At the first step of measurement, interactively determined representative regions (square sampling) in these structures (glial cells 30 × 30 pixels, neurons 60 × 60 pixels, neuropil 120 × 120 pixels) were analysed. These frames lie completely within the SOIs. Therefore, a correction due to the Schwarzschild–Villinger effect, in order to eliminate illumination errors at the border of small objects, is not necessary. Only those stainings with large contrasts were remeasured using larger sample sizes. All measurements were performed in the center of the object screen where the geometrical distorsion is minimal. After the shading correction of each gray value transformed color image the specific analysis was started. The computation of the maximum of contrast C was performed as follows:

$$C=\frac{\frac{\|\overline{R_i^4}-\overline{R_n^4}\|+\|\overline{R_i^4}-\overline{R_g^4}\|}{2}+\frac{\|\overline{G_i^4}-\overline{G_n^4}\|+\|\overline{G_i^4}-\overline{G_g^4}\|}{2}+\frac{\|\overline{B_i^4}-\overline{B_n^4}\|+\|\overline{B_i^4}-\overline{B_g^4}\|}{2}}{3}.$$

The variables R, G and B are the mean gray values of a SOI. The indices i, n and g indicate the R, G and B values of the neuropil, the neurons and the glia SOIs, respectively. Finally, $\overline{R^4}$ is the mean gray value (similiar calculations would be performed for $\overline{G^4}$ and $\overline{B^4}$) in a defined closed $X \times Y$ region (r) of pixels with 4 vertices (quadrant sampling) (Fig. 1) where each pixel has a brightness of $b(x,y)$:

$$\overline{R^4}=\frac{1}{r}\times\sum_{i=1}^{r}b(x;y).$$

The fine measurement of C_f was performed in n randomized neurons, glial cells and neuropil.

$$C_f=\frac{\frac{\overline{\|R_i^p-R_n^p\|}+\overline{\|R_i^p-R_g^p\|}}{2}+\frac{\overline{\|G_i^p-G_n^p\|}+\overline{\|G_i^p-G_g^p\|}}{2}+\frac{\overline{\|B_i^p-B_n^p\|}+\overline{\|B_i^p-B_g^p\|}}{2}}{3}.$$

The regions were polygonal (index p with $p>4$ vertices), corresponding to the contour of glial cells and neurons (polygonal sampling) (Fig. 1). The numerical expression for the mean $\overline{C_f}$ of C_f is simply

$$\overline{C_f}=\frac{1}{n}\times\sum_{i=1}^{n}C_{f_i}.$$

In order to find a measure for the differentiation of structures, the standard deviation (V) of gray values in each color channel and its mean $\overline{V_f}$ of SOIs were used.

$$V=\frac{\frac{\overline{\|Rv_i^4-Rv_n^4\|}+\overline{\|Rv_i^4-Rv_g^4\|}}{2}+\frac{\overline{\|Gv_i^4-Gv_n^4\|}+\overline{\|Gv_i^4-Gv_g^4\|}}{2}+\frac{\overline{\|Bv_i^4-Bv_n^4\|}+\overline{\|Bv_i^4-Bv_g^4\|}}{2}}{3},$$

$$V_f=\frac{\frac{\overline{\|Rv_i^p-Rv_n^p\|}+\overline{\|Rv_i^p-Rv_g^p\|}}{2}+\frac{\overline{\|Gv_i^p-Gv_n^p\|}+\overline{\|Gv_i^p-Gv_g^p\|}}{2}+\frac{\overline{\|Bv_i^p-Bv_n^p\|}+\overline{\|Bv_i^p-Bv_g^p\|}}{2}}{3},$$

$$\overline{Rv^4}=\sqrt{\frac{\sum_{i=1}^{r}(b_i(x;y)-\overline{b_i(x;y)})^2}{r}},$$

$$\overline{V_f}=\frac{1}{n}\times\sum_{i=1}^{n}V_i.$$

A very important feature of a certain staining method is its constancy in different brain regions. Therefore, the local contrasts of fine measurements of the striatum and the hippocampus were compared and the measure is called O [%] (optimum value). An optimum value is given if the local contrast and the similarity ΔC is high. That means the contrast difference in the hippocampus, C_h, and striatum, C_s, is small, but the contrast is large and the variability of the SOIs in the color channels is large, too.

$$\Delta C=\|\overline{C_s}-\overline{C_h}\|,$$

$$O=\frac{\frac{\overline{C_s}+\overline{C_h}}{2}+100-\Delta C}{2}.$$

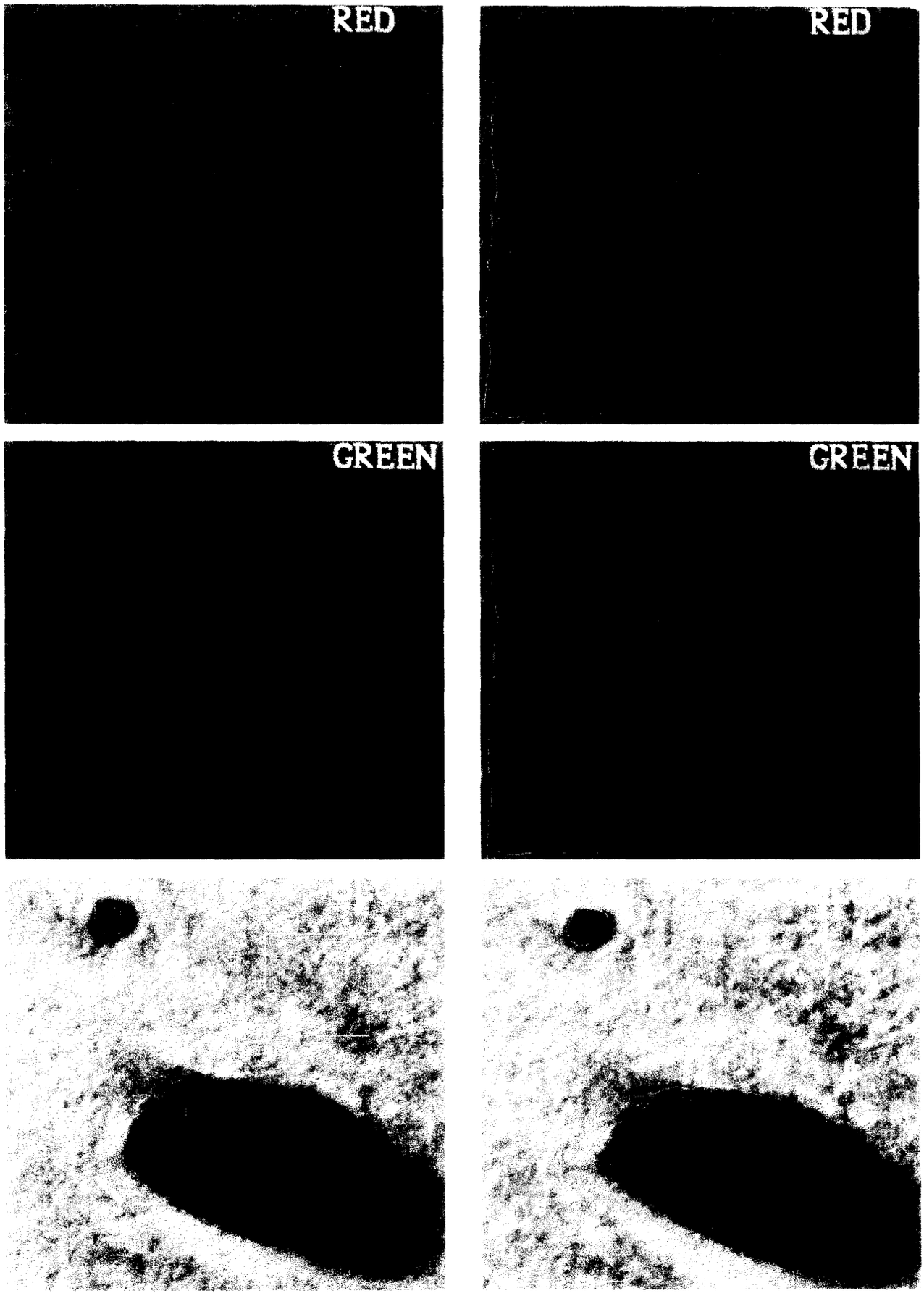

Fig. 1. Sampling schemes in the three color channels. Left: frame measurements. Right: polygonal regions of fine measurements according to the contours of SOIs.

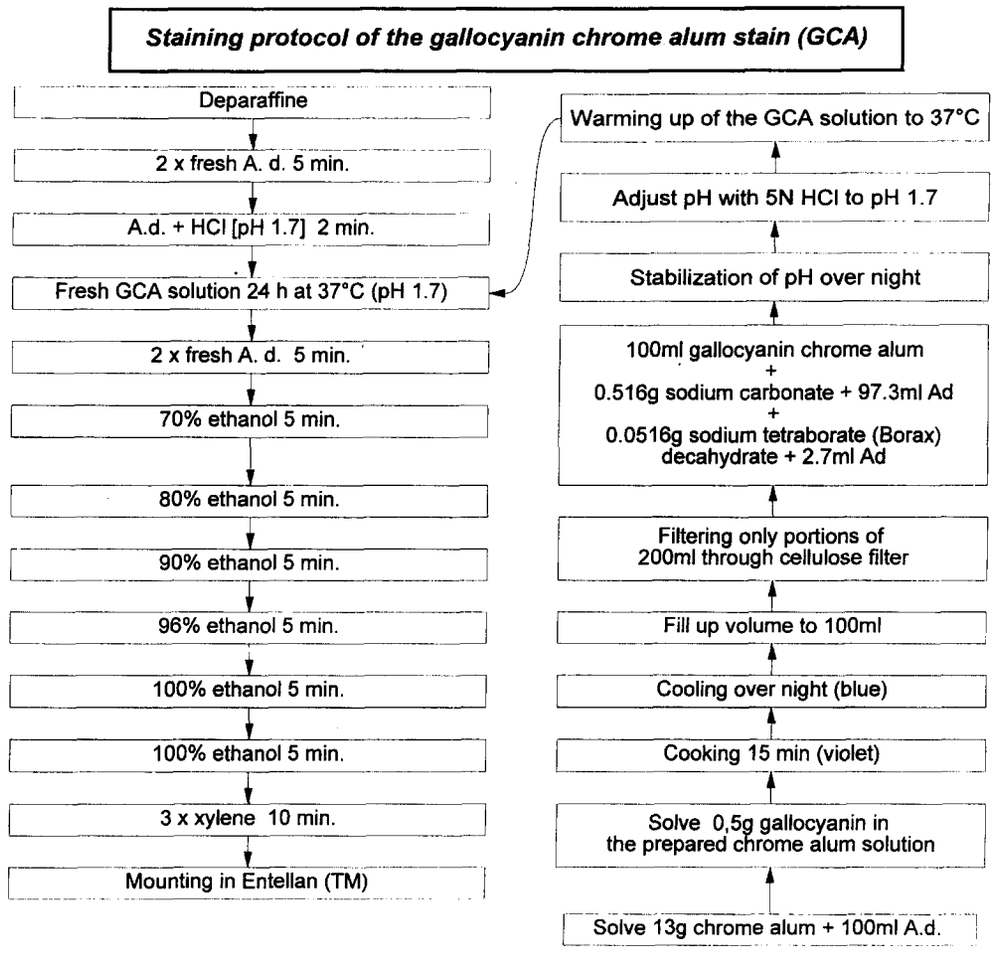

Fig. 2. Staining procedure which has given the optimal staining for image analysis.

RESULTS

For the final results, the contrast and constancy of the stains were taken into account because for all stains providing a high contrast level (>30%), nucleoli, caryoplasm and cytoplasm are differentiable. The costs are negligible because using dyes is 20 to 40 times cheaper than using commercial antibodies which react with epitopes on glial cells or neurons. No staining times are longer than 24 h.

In the summarizing Fig. 5, an overview of all contrast values of neurons and glial cells in the neostriatum and hippocampus is given. Some specific contrast curves intersect the mean neostriatum and hippocampus graph. At these intersections the relation of higher contrast in the striatum and lower contrast in the hippocampus is inverted. The contrast variations between glial cells and neurons can be judged here.

In Fig. 6 and Fig. 7, only those stains which, respectively, reached contrast and optimum contrast values greater than 29% and 55% were plotted. The stain found to have the highest contrast and constancy is a modification of the gallocyanin chrome alum stain. The optimum value of this stain is 74% analysed in quadrant samples. However, using a polygonal sample in combination with a sample size of 100 neurons, glial cells and neuropil regions (300 SOIs), the contrast is reduced to 42% (Fig. 8). All other high contrast stains show a similar decrease of their contrast values within polygon sampling because this measurement collects more gray values within the lighter stained cytoplasms. Nevertheless, these values are more precise. Gallocyanin chrome alum staining shows a clear and regular impregnation of SOIs throughout the striatum and the hippocampus (Fig. 14). A detailed description of optimal gallocyanin chrome alum staining is shown in Fig. 2. The Fe^{3+} chelate of the dye was introduced by Proescher and Arkush (1928) and the Cr^{3+} chelate by Einarson (1932). An important step in the preparation of the dye is the heating of chrome alum with gallocyanin for a minimum of 15 min at 100°C. In this time the actual histochemical active dye complex, a Cr^{3+} chelate, is produced. The structure of the amphoteric oxazine dye is substituted by carboxylate and dimethylamine groups within the reaction in hot aqueous solution in the presence of a chromium (III) salt. Therefore, the staining solution contains a gallocyanin chrome alum complex in a relation of 2:1. This dye complex is stable for about 14 days at RT. After 20 to 28 days the staining intensity of the complex decreases. The composition of the dye solution in Fig. 2 has been determined systematically by contrast measurements which are not shown here. The optimal procedure of the stain is shown in Fig. 2. The pH optimum of the staining solution is 1.7 and was adjusted

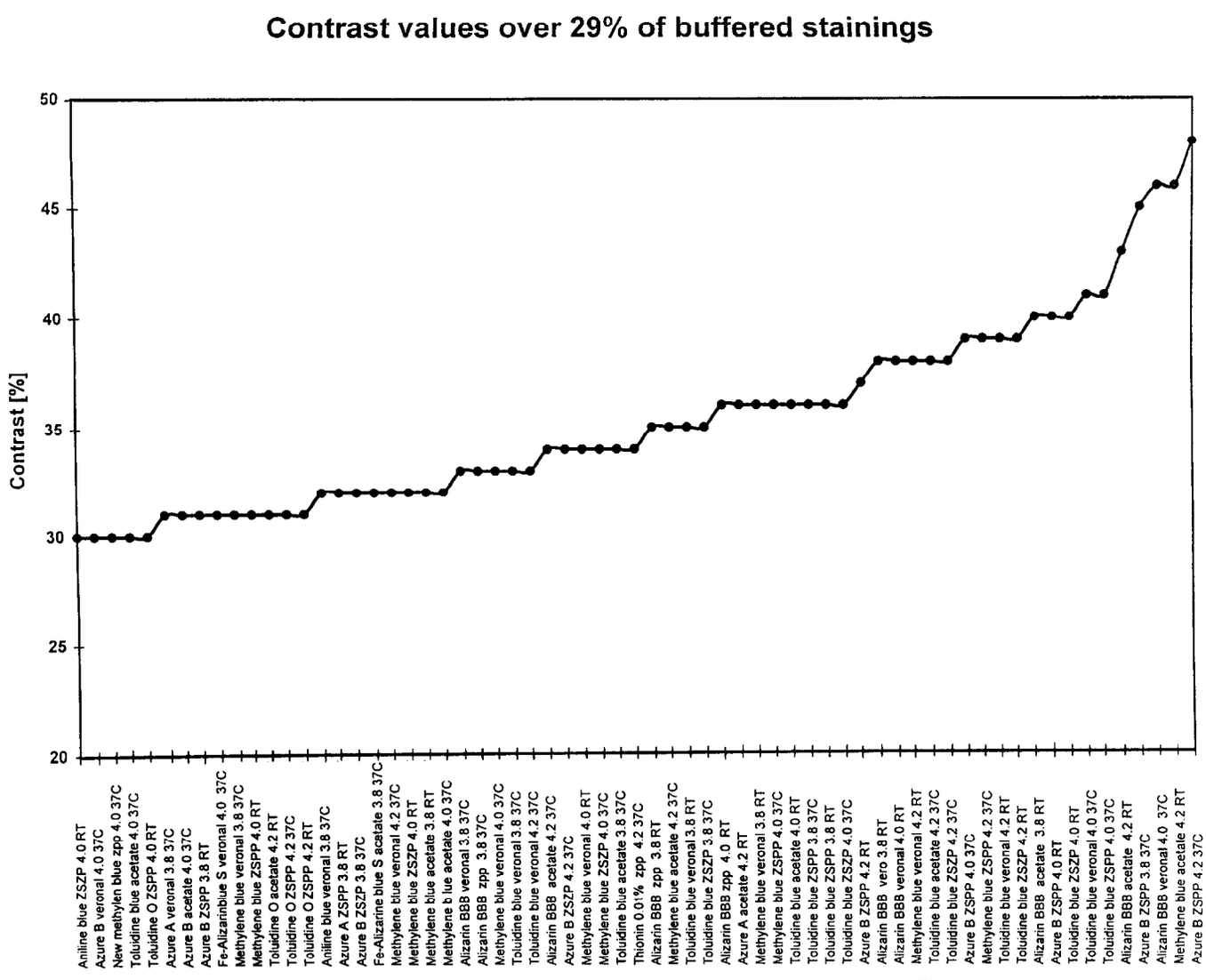

Fig. 3. Sorted contrast values of those stainings in different buffer systems which are larger than 29%. The contrasts are based on the mean of glial cell and neuron to neuropil color differences.

with a 5N HCl solution. Only one filter should be used for a volume of approximately 200 ml of the gallocyanin chrome alum solution. Staining at room temperature does not produce as much background staining as at 37°C.

The standard cresyl violet stain has the same contrast value as the thionin stain and lies within the upper range of contrasts. The measurements using square sampling are not as precise as those of polygonal sampling, but they represent a significant range of contrast which generally persists within polygonal sampling. For final measurements polygonal sampling can be recommended.

Aqueous staining solutions which show higher contrasts and higher constancies were investigated by systematic pH (3.8, 4.0, 4.2) and temperature (room temperature and 37°C) modifications (Fig. 3). This pH range was established after testing pHs between 2.5 and 7.0. Only the small range between 3.8 and 4.2 leads to reasonable staining results. Altogether, eleven stains were investigated systematically by temperature and pH variation with respect to their differences in contrast between buffered and non-buffered staining media (Table 2).

The optimum value of these stains is obtained by application of iron alizarine blue S in acetate buffer (pH 3.8) incubated at 37°C. A selection of optimum values over 60% is given by Fig. 4. Basic thiazine dyes like methylene blue, toluidine O, new methylene blue, and acid anthrachinon dyes like iron alizarin blue S and alizarin blue black B within a pH of 3.8 and 4.0 have given maximal results within the group of buffered stainings.

Alcohol solution stains were modified according to dye concentrations and incubation times. Generally, the contrast of dye solutions in alcohol media is lower than that obtained with the dyes in aqueous solutions. For this reason, the results of alcohol solutions are not presented in detail.

Most methods are based on procedures documented in the literature. It was often necessary to modify and optimize them for the neurohistological application.

Finally, different system components which influence contrast were investigated by using an optimized sample of the gallocyanin chrome alum staining. These were light intensity, the signal amplification capabilities of the camera and the filtered wavelengths. An important

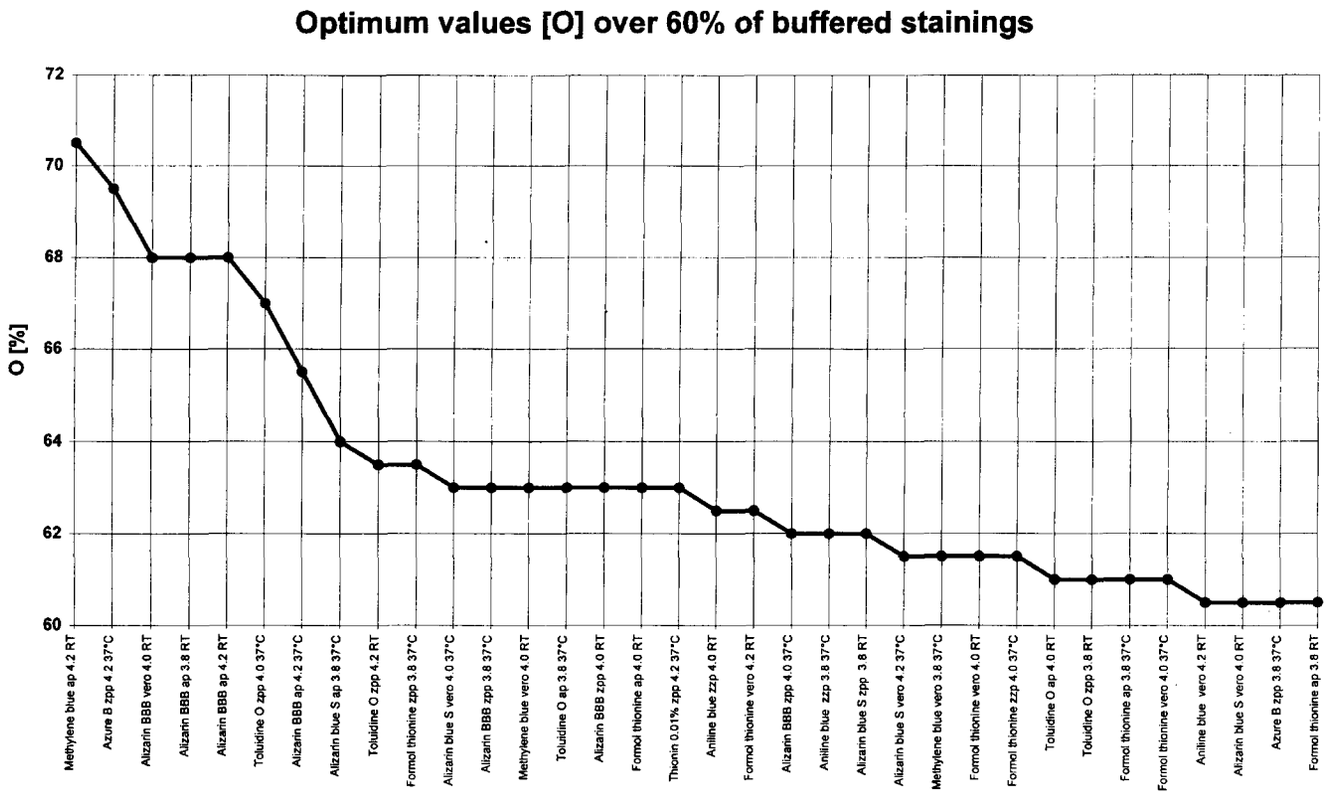

Fig. 4. The optimum values of stains in buffer systems which are larger than 60% are summarized in this diagram (RT: room temperature, ZSPP: citric acid phosphate buffer, VERO: veronal acetate buffer, AP: acetate buffer, ZPP: citric acid phosphate buffer). The number behind the names of the stains indicate the pH value of the buffer.

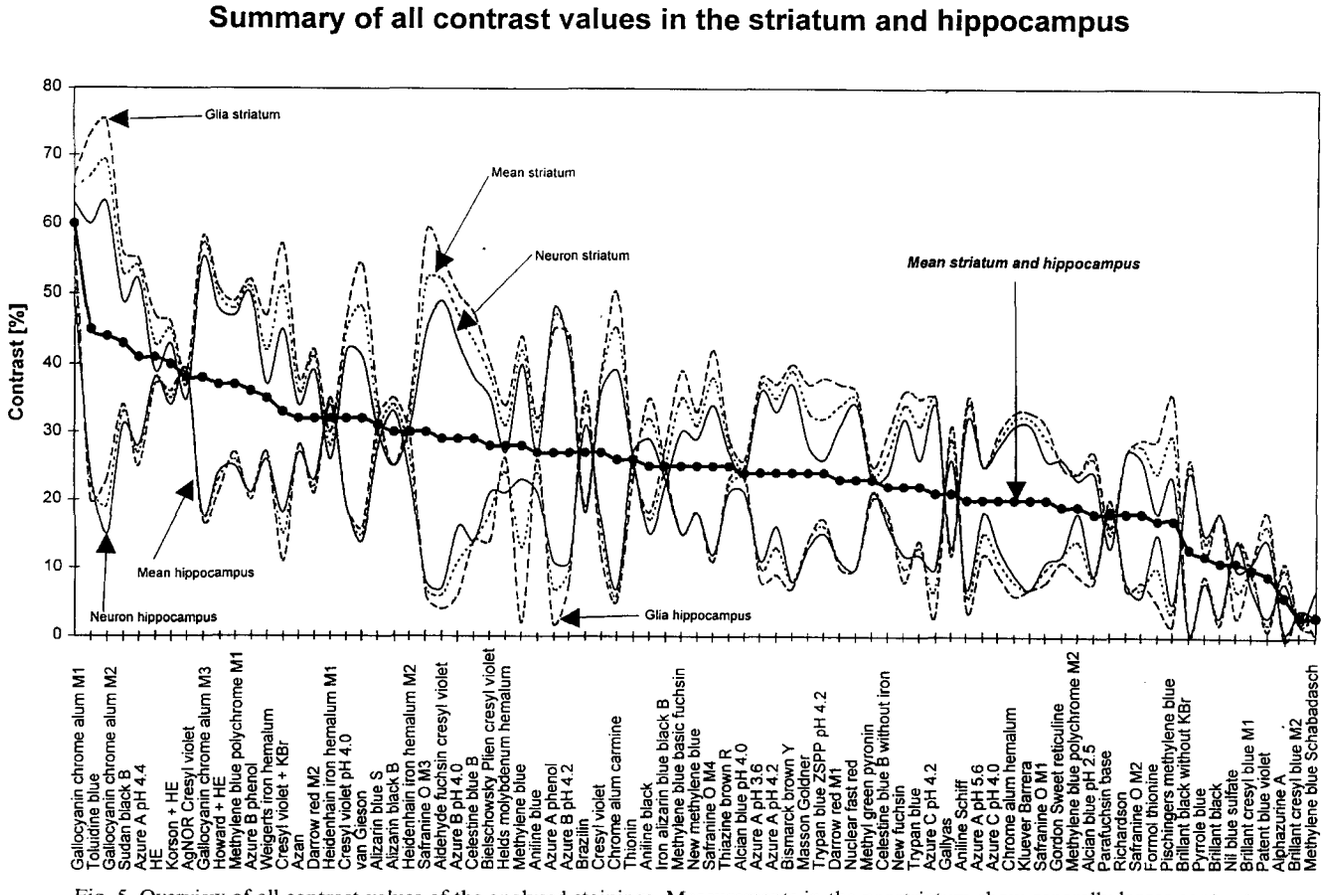

Fig. 5. Overview of all contrast values of the analysed stainings. Measurements in the neostriatum show generally larger contrast values (upper three curves). The lower three curves are contrast results of the hippocampus. The thick curve between them indicates the mean of all measurements in the different structures.

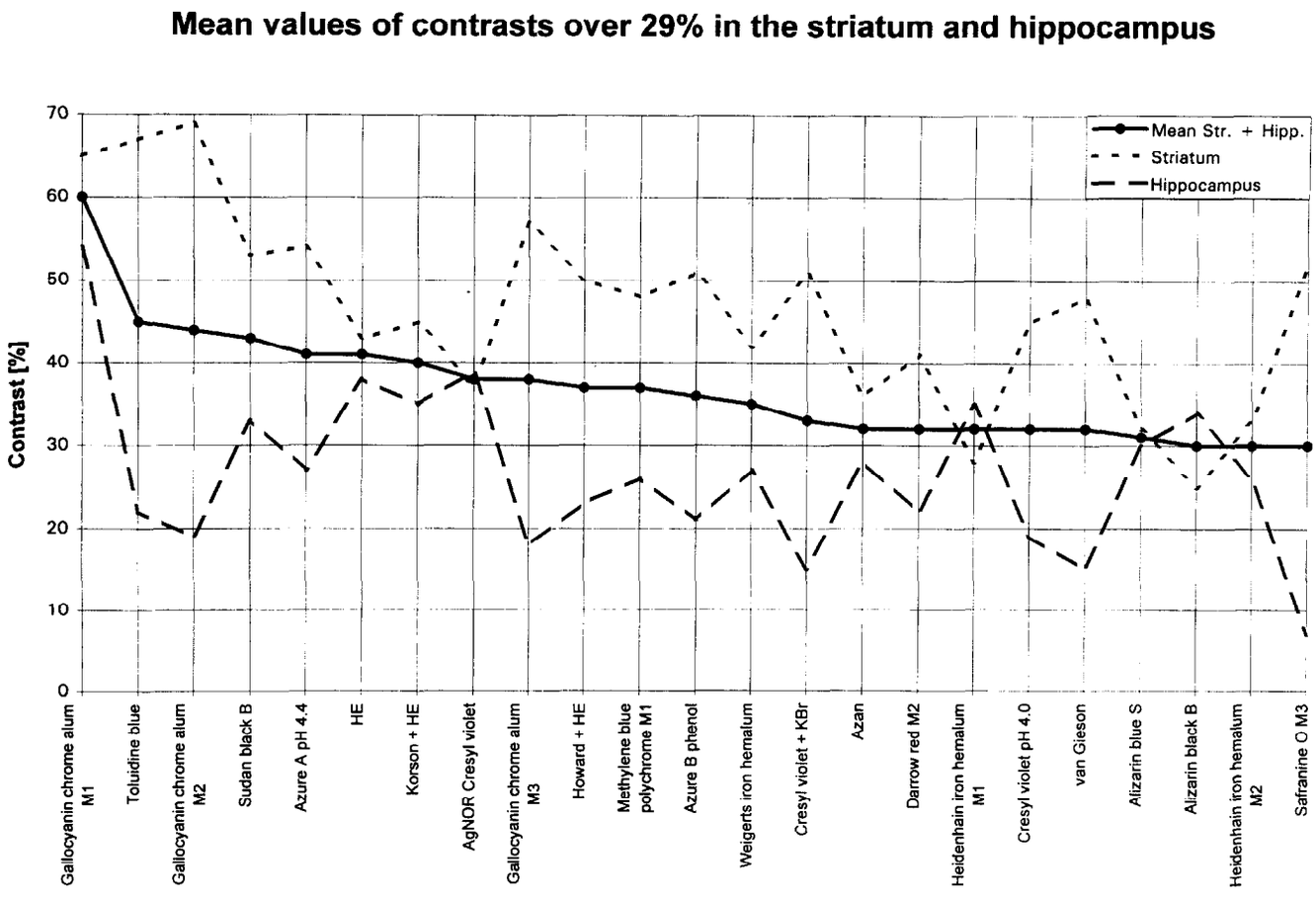

Fig. 6. Comparison of mean contrasts which exceed 29% in the striatum and hippocampus.

feature of the camera is its programmable resolution and the selection of a certain range of transmitted bits. This range is dependent on the object and light intensity. Therefore, a determination was performed to find out which are the most significant bits or the optimal gain setting. Using 12 linear, a root and one logarithmic ranges of the gain, the contrast values were plotted within a modification of the voltage of the light source. Fig. 9 shows that a maximum contrast of 41% can be achieved by using 5.8 V at the light source and gain 6 of the camera amplification range.

For the determination of the optimal wavelength filter, the gray level video camera K30 from Siemens was used. Before the measurement of contrast of a specified SOI at a certain wavelength is performed, the light intensity at each filter position and for each wavelength must be calibrated to a defined (in this case 111) mean gray value of the digitized image to insure that each image has nearly the same mean gray value (Fig. 10). Using the same adjustments as shown in Fig. 10, the contrast of SOIs is plotted against the filtered wavelengths from 490 nm to 630 nm. The maximum contrast lies between 560 nm and 580 nm (Fig. 11). This correlates with the larger part of the relative spectral response of the ProgRes camera for the green channel which lies between 500 nm and 570 nm. This indicates that it is possible to measure the most significant amount of information with respect to contrast of the gallocyanin chrome alum staining within one color channel.

A further important factor which influences the contrast of a stain is the section thickness. An increasing section thickness leads to a decrease of the contrast (Fig. 12). The contrast values in a gallocyanin chrome alum stained section series ranging in thickness from 4 μm to 50 μm was determined. A contrast decrease begins at a section thickness of about 28 μm. This also depends significantly on SOI density. A high SOI density in a section reduces the contrast more than a small SOI density of a section with the same thickness because the absorption of light and structures overlapping each other increase within higher SOI densities. This leads to the problem of strongly variable SOI densities in large sections, e.g. high densities in the molecular layer of the cerebellum and low densities in the layer one of the isocortex.

Lastly, the staining time with respect to the contrast was evaluated. Contrasts were determined within 20 min to 48 h of staining (Fig. 13) in 12 μm thick sections. It was found that between 12 and 28 h of incubation the contrast stays nearly constant.

DISCUSSION

Systematic quantifications of staining results are an important step in the direction of serious quality control in histochemistry. Furthermore, it is an objective

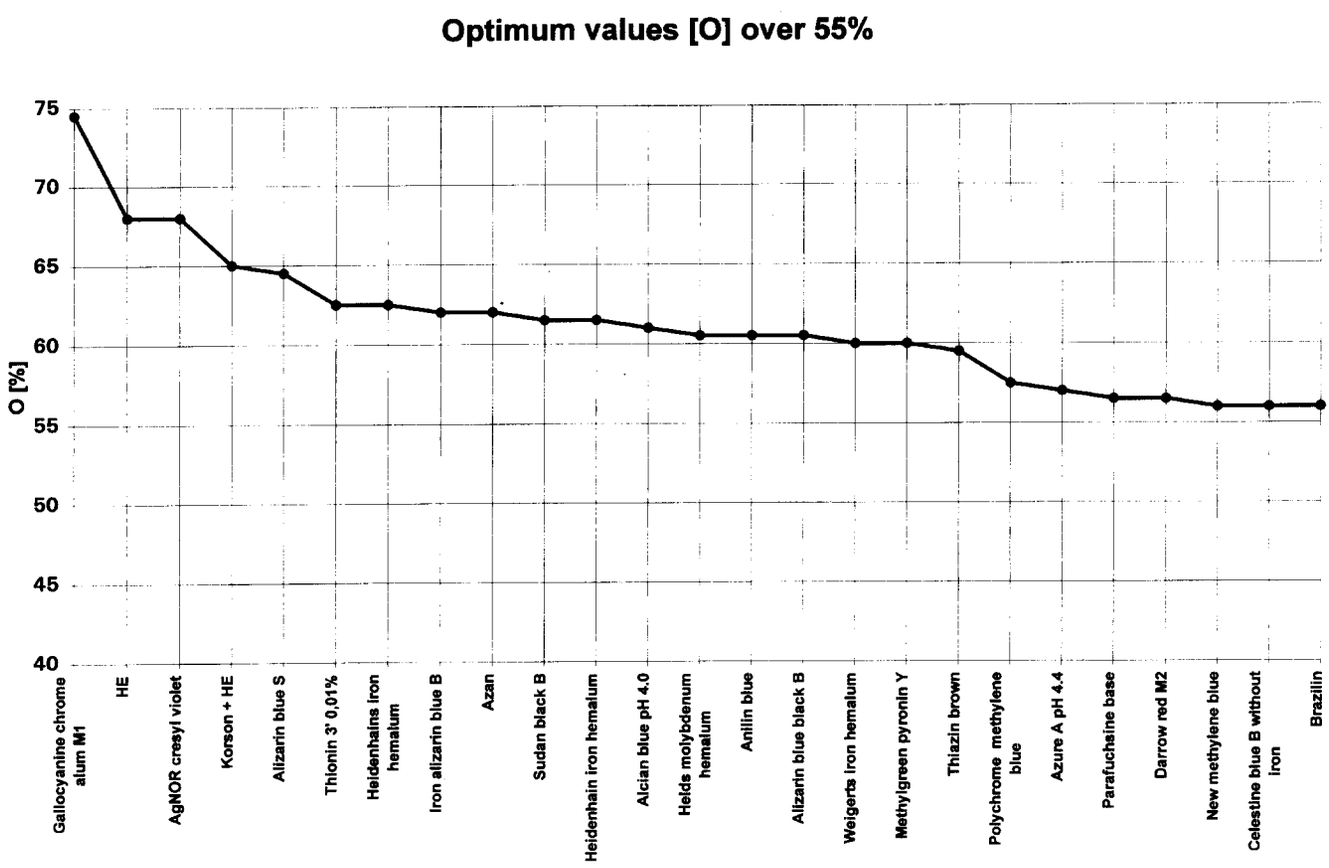

Fig. 7. Plot of the optimal stainings over 55%.

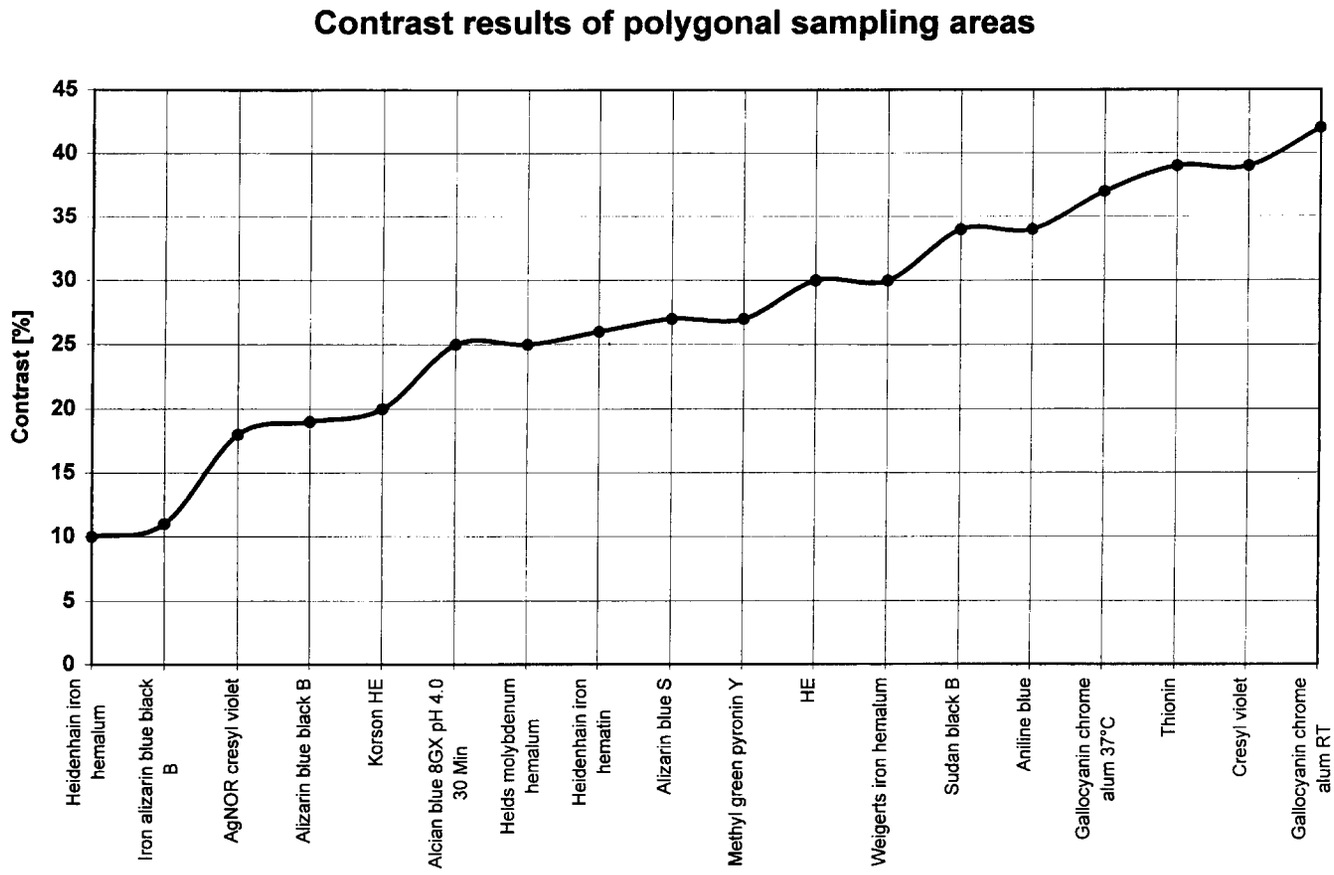

Fig. 8. Contrasts of polygonal sampling of 300 evaluated SOIs within every staining.

Table 2. Results of maximal contrast measurements before and after the application of buffer systems

Staining	Contrast without buffer (%)	Buffer system	pH	Temperature (°C)	Contrast with buffer (%)
Alizarin blue black B	30	veronal buffer	4.0	37	46
Aniline blue	27	veronal buffer	3.8	37	32
Azure A	24	acetate buffer	4.2	37	36
Azure B	27	citrate phosphate buffer	4.2	37	48
Iron alizarin blue S	31	acetate buffer	3.8	37	32
Methylene blue	28	acetate buffer	4.2	RT	46
New methylene blue N	25	citrate phosphate buffer	4.0	37	30
Toluidine blue	45	citrate phosphate buffer	4.0	37	41
Trypan blue	22	acetate buffer	4.0	RT	15
Formol thionine	17	citrate buffer	3.8	37	29
Thionine 0.01%	26	citrate buffer	4.2	37	34
Mean	27				35

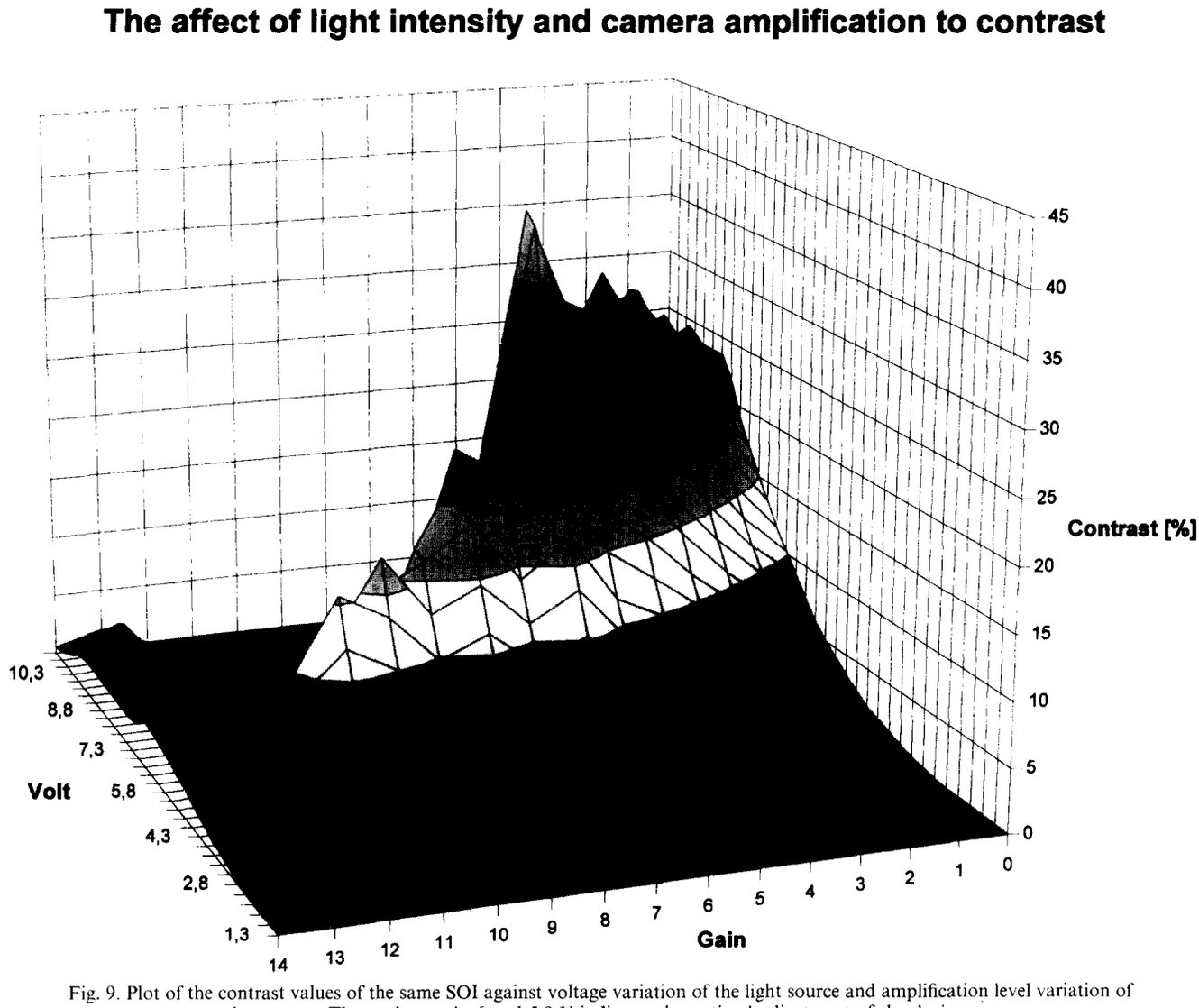

Fig. 9. Plot of the contrast values of the same SOI against voltage variation of the light source and amplification level variation of the camera. The peak at gain 6 and 5.8 V indicates the optimal adjustment of the devices.

method to decide which staining procedure is optimal for a distinct problem solvable by image analysis.

The high-resolution ProgRes 3012 camera offers the possibility to measure the transmission of certain colors after having passed the absorbing section. Three-color photometers (Taylor *et al.*, 1978) or sliding interference filters (Aus *et al.*, 1976, 1977; Cheng, 1974; Aggarwal and Bacus, 1977; Piller, 1977) are unnecessary for this application. The measurement is performed within programmable resolutions in single color channels. This equipment makes it possible to determine the contrast of stainings in an objective way. A disadvantage of the RGB CCD cameras is that the spectral band cannot be modified like a sliding interference or monochrome filter.

The comparability of the contrast values with other measurements is only problematic with respect to the determination of light intensity and the camera gain. To

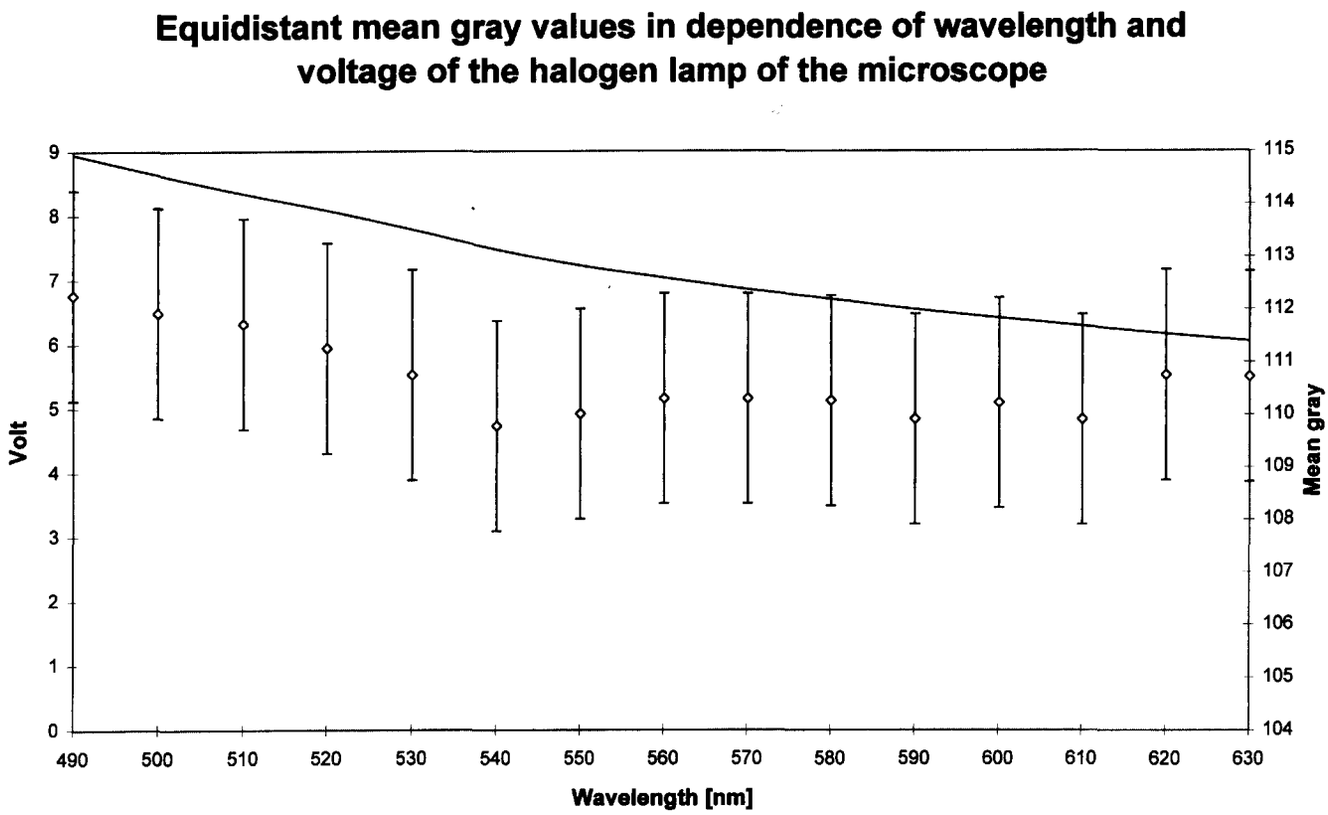

Fig. 10. The variation of wavelength and light intensity by changing the voltage of the light source should approximately result in the same mean gray level of an image with SOIs. This indicates a stable measurement system with respect to CCD camera sensitivity (wavelength) and light intensity (V). The mean gray levels (open rhombus) lie between 112.5 and 109.5, which is considered a tolerable variation.

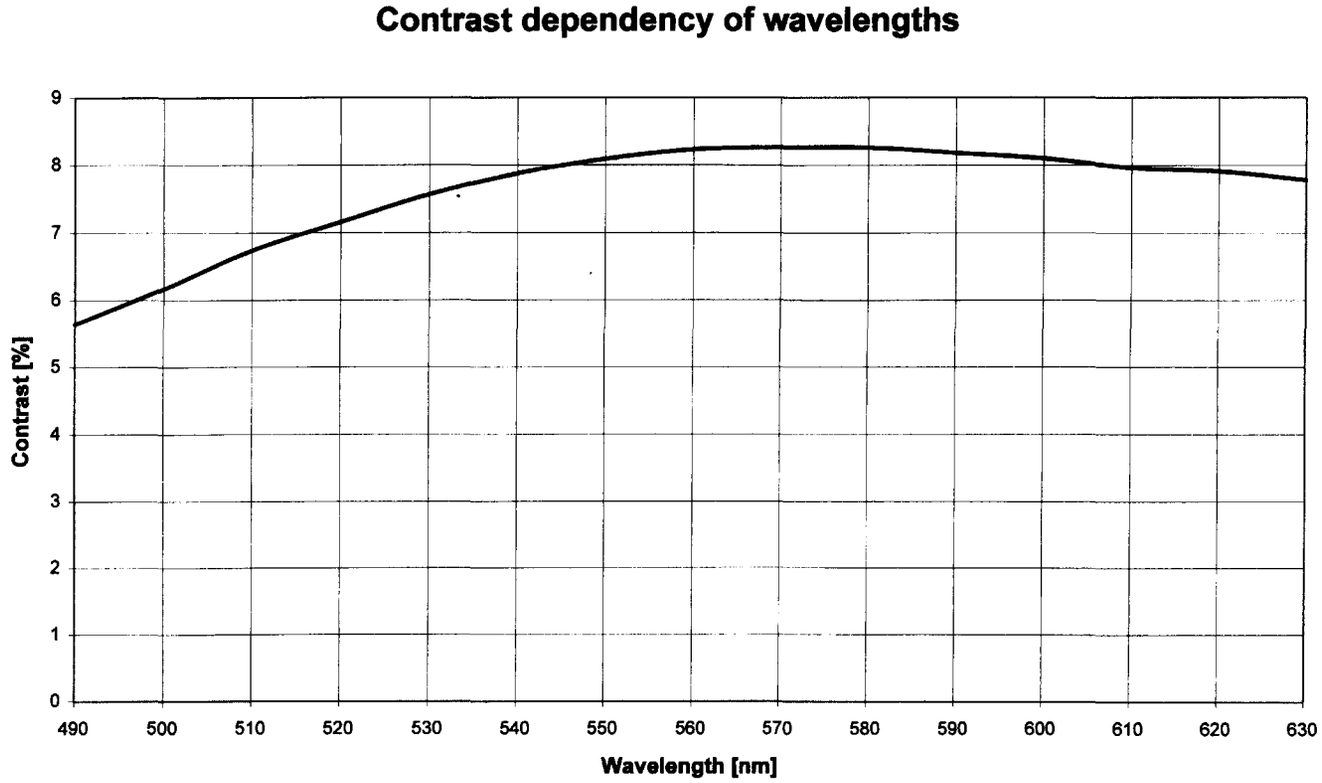

Fig. 11. Within the tolerable variation of mean gray levels the contrasts of SOIs at different wavelengths using a monochrome filter were calculated. For this measurement a gray level camera (K30 Siemens®) was used. Maximum contrast can be reached using a filter wavelength between 560 and 580 nm.

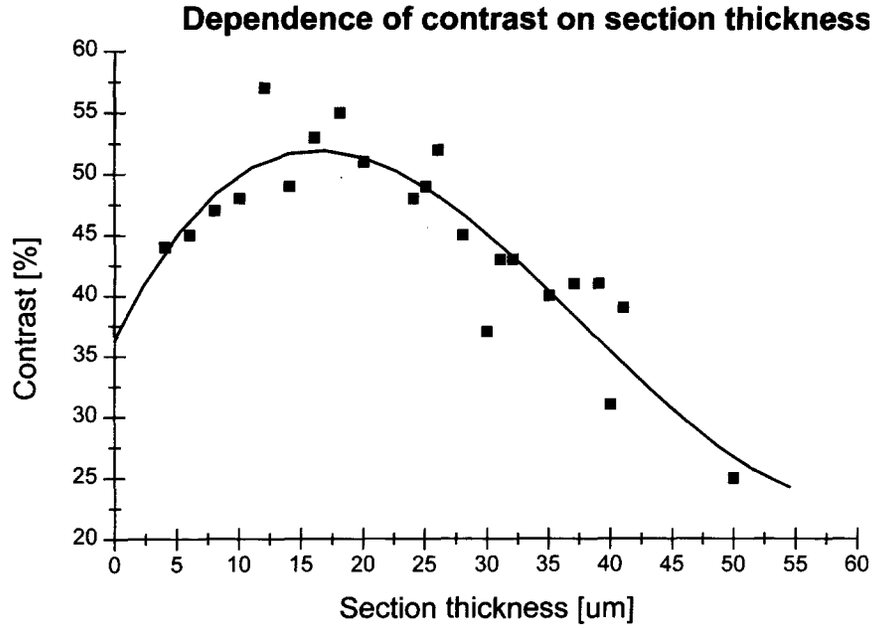

Fig. 12. Contrast measurements at different section thicknesses. The contrast values vary slightly over section thicknesses between 6 and 28 μm.

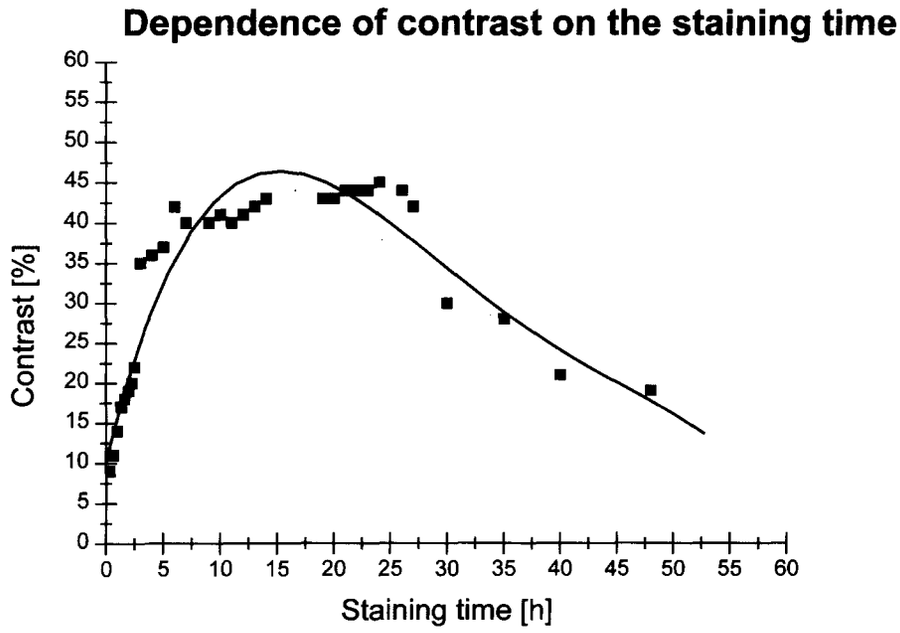

Fig. 13. Contrast measurements at different staining times. The contrast values are nearly constant within a staining time between 5 and 30 h. This is a good feature of the gallocyanin chrome alum staining because the contrast is relatively stable over a wide range of staining time.

minimize this problem of comparability, a calibration of the whole system should be performed at the beginning of any measurement. This includes the determination of light intensity contrast curves, wavelength contrast curves and, if possible, finding out the maximum contrast within a certain gain setting. If the measurements of contrast are performed in an optimally adjusted measurement system, their results should be comparable with other optimized measurement systems. The use of relative or normalized contrast values simplifies comparisons. If the color information from the SOIs of one staining is strongly contrasted, for example glial cells are stained blue, neurons are stained green and the neuropil is stained allover red, it then makes sense to normalize the color information by a LUT transformation into the CIE-XYZ system as proposed by Wölker (1993).

Due to the similarities of computation there were no differences in the contrast values between the mean optical density (MOD) or integrated optical density (IOD) and the mean gray values of the SOIs (Bradbury, 1983; Lyon *et al.*, 1989; Salmon *et al.*, 1994; Kiss *et al.*, 1991, 1992, 1993; Zandona *et al.*, 1994). Therefore, the MOD and IOD measures were not used here.

Irregularities in staining are often caused by different dye contents and by the manufacturing of dyes as discussed in Wittekind (1981) and Yemma and Penza (1987). The qualities of dyes might be analysed by using the same method as described above instead of the

Fig. 14. Photomicrographs showing results of the gallocyanin chrome alum staining. (A) Staining of the neostriatum (700 ×). The large open arrow indicating a medium-sized neuron. Glial cells (small open arrow) are clearly distinguished from the background. A large neuron is shown here, too (large solid arrow). (B) Staining of the hippocampus (1200 ×). The appendages of neurons are stained, too. (C) The cytoplasms of neurons (solid arrow) in the CA1 region are stained intensively but the neuropil is nearly unstained (700 ×). (D) Glial cells (solid arrow) are stained clearly all over the hippocampus. The contrast between the caryoplasms and background is very high (700 ×).

chemical determination of the dye content of a substance. Consequently, dye concentrations must be modified in order to get maximal contrasts.

The contrast of different staining procedures was investigated only in the CNS material of humans. Further measurements have to be done in other tissues and species.

Mainly those stains which stain nuclei were applied. Because the neuropil consists of a large amount of neuronal and glial cytoplasm, axon and dendrite stains would enhance the staining of the background, and consequently reduce the contrast. Nucleus stains imply a more or less specific staining of DNA elements which are basophilic. So, the stains with high contrasts are based on basic dyes in an acidic buffer or an alcohol solution.

Of course, there are many other brain regions which can be measured in order to verify the constancy of a certain staining procedure. However, the question is which staining procedure is good enough to be considered for such investigations. Now the decision is easier because only those stains with a certain well-known optimum value need be taken into account. For example, only 4 procedures remain with an optimum value over 64%: Korsons silver staining (Korson, 1964) in combination with cresyl violet, the AgNOR cresyl violet procedure, the hemalum chrome alum technique and the gallocyanin chrome alum method.

The highest contrast and constancy results were obtained using the oxazine gallocyanin in combination with the inorganic components chrome alum and sodium tetraborate in an aqueous incubation medium. Given our findings, gallocyanin chrome alum can be strongly recommended as the gold standard of CNS staining for efficient MUR LIA analysis.

Acknowledgements—The authors wish to thank Mrs Almert and Mrs Schubert for their excellent technical assistance.

REFERENCES

Aggarwal, R. K. and Bacus, J. W., 1977. A multi-spectral approach for scene analysis of cervical cytology smears. *Journal of Histochemistry and Cytochemistry*, **25,** 668–680.

Agnati, L. F., Fuxe, K., Janson, A. M., Zoli, M. and Härfstrand, A., 1986. Quantitative analysis: computer-assisted morphometry and microdensitometry applied to immunostained neurons. In *Immunocytochemistry. Modern Methods and Applications*, eds J. M. Polak and S. Van Noorden, pp. 205–224. Wright, Bristol.

Ahrens, P., Schleicher, A., Zilles, K. and Werner, L., 1990. Image analysis of Nissl-stained neuronal perikarya in the primary visual cortex of the rat: automatic detection and segmentation of neuronal profiles with nuclei and nucleoli. *J. Microsc.*, **157,** 349–365.

Albert, R., Schindewolf, T., Müller, J. and Harms, H., 1993. Ein bildanalytisches Verfahren zur Bestimmung dreidimensionaler morphometrischer Gewebestrukturmerkmale im Lichtmikroskop. In *Informatik aktuell Mustererkennung 1993*, eds S. J. Pöppl and H. Handels, pp. 399–406. Springer, Berlin.

Amunts, K., Istomin, V. and Schleicher, A., 1995. Postnatal development of the human primary motor cortex: a quantitative cytoarchitectonic analysis. *Anat. Embryol.*, **192,** 557–571.

Aus, H. M., Gunzer, U. and Meulen, V. T., 1976. A note on the usefulness of multi-color scanning and image processing in cell biology. *Microscope*, **24,** 39–48.

Aus, H. M., Rüter, V., Meulen, V. T., Gunzer, U. and Nürnberger, R., 1977. Bone marrow cell scene segmentation by computer-aided color cytophotometry. *Journal of Histochemistry and Cytochemistry*, **25,** 662–667.

Berios, M., 1995. Anti-fading agents for confocal immunofluorescence: colocalization of nuclear polypeptides. *Biotech. Histochem.*, **70,** 40–45.

Berkowitz, L. R., Fiorello, O., Kruger, L. and Maxwell, D. S., 1968. Selective staining of nervous tissue for light microscopy following preparation for electron microscopy. *Journal of Histochemistry and Cytochemistry*, **16,** 808–814.

Böck, P., 1979. Improved Nissl method to stain formaldehyde- or glutaraldehyde-fixed material. *Acta Neuropath.*, **46,** 243–244.

Braak, H., 1984. Architectonics as seen by lipofuscin stains. In *Cerebral Cortex*, eds A. Peters and E. G. Jones, Vol. 1, pp. 59–104.

Braak, H., 1988. Silver impregnation of Alzheimer's neurofibrillary changes counterstained for basophilic material and lipofuscin pigment. *Stain Technology*, **63,** 197–200.

Bradbury, S., 1983. Commercial image analysers and the characterization of microscopical images. *J. Microsc.*, **131,** 203–210.

Camby, I., Salmon, I., Danguy, A., Pasteels, J. L. and Kiss, R., 1995. The use of the digital cell image analysis of Feulgen-stained nuclei to detect apoptosis. *Histochem. Cell. Biol.*, **104,** 407–414.

Capowski, J. J., 1989. *Computer Techniques in Neuroanatomy*. Plenum Press, New York.

Cheng, G. C., 1974. Color information in blood cells. *Journal of Histochemistry and Cytochemistry*, **22,** 517–521.

Clark, G. and Clark, M. P., 1971. *A Primer in Neurological Staining Procedures*. Springfield.

Clark, G., 1973. *Staining Procedures Used by the Biological Stain Commission*, p. 89. Baltimore.

The Colour Index 1971 ed. The American Association of Textile Chemists and Colorists. Bradford, 1971.

Decaesteck, C., Remmelink, M., Camby, I., Salmon, I., Goldschmidt, D., Van Ham, P., Pasteels, J. L. and Kiss, R., 1995. The combination of a decision tree technique with the computer-assisted microscope analysis of Feulgen-stained nuclei to assess aggressiveness in lipomatous and smooth muscle tumors. *Anticancer Research*, **15,** 1311–1317.

Deutsche Chemische Gesellschaft, 1935. *Beilsteins Handbuch der organischen Chemie*, Vol. 21, p. 438. Springer, Berlin.

Deutsche Chemische Gesellschaft, 1953. *Beilsteins Handbuch der organischen Chemie*, Vol. 21, p. 330. Springer, Berlin.

Deutsches Institut für Normung e.V., 1993. DIN 5033-Farbmittel, Vol. 49, p. 12. 4th edn. Beuth, Berlin.

Duckett, S. and Triggs, M., 1965. Silver iodate techniques for the histological demonstration of normal and pathological nervous tissue. *J. Royal Microsc. Soc.*, **84,** 485–488.

Eggers, R., 1990. Triple staining of brain tissue for neuronal classification. *Z. Mikrosk.-Anat. Forsch.*, **104,** 55–60.

Eichler, V. B. and Taylor, P. W., 1976. A new metachromatic stain technique for paraffin-embedded neural tissue using thionine. *J. Microsc.*, **108,** 97–99.

Einarson, L., 1932. A method for progressive selective staining of Nissl and nuclear substances in nerve cells. *Am. J. Path.*, **8,** 295–307.

Eins, S., 1973. Anwendung der automatischen Bildanalyse auf dem Gebiet der Neuroanatomie. *Fortschritte der quantitativen Bildanalyse*, IMANCO Symposium, pp. 43–51.

Eins, S., 1974. Automatic image analysis in the medical and biological sciences. *Microscope*, **22,** 59–68.

Eins, S. and Wilhelms, E., 1976. Assessment of preparative volume changes in central nervous tissue using automatic image analysis. *Microscope*, **30,** 29–38.

Eins, S. and Gallyas, F., 1977. Selektive und kontrastreiche Färbungen im Hirngewebe. *Microscopica Acta*, **Suppl 1,** 157–164.

Eins, S. and Gallyas, F., 1978. Möglichkeiten der automatischen Bildanalyse von Hirngewebe nach Silberimprägnierung. *Verh. Anat. Ges.*, **72,** 407.

Fischer, R., Zeman, W. and Irons, I., 1961. Differential dye-uptake in excited and non-excited nervous tissue after treatment with pepsin and neotetrazolium chloride. *Journal of Histochemistry and Cytochemistry*, **9,** 103.

Foley, J. D., van Dam, A., Feiner, S. K., Hughes, J. F. and Phillips, R. L., 1994. *Einführung in die Computergraphik*, pp. 447–478. Addison-Wesley, Bonn.

Forbes, D. A. and Petry, R. W., 1979. Computer-assisted mapping with the light microscope. *J. Neurosc. Meth.*, **1,** 77–94.

Gabe, M., 1976. *Histological Techniques*. Masson, Paris.

Gallyas, F., 1993. Four modified silver methods for thick sections of formaldehyde-fixed mammalian central nervous tissue: "dark" neurons, perikarya of all neurons, microglial cells and capillaries. *J. Neurosci. Meth.*, **50,** 159–164.

Giloh, H., 1982. Fluorescence microscopy: reduced photobleaching of rhodamine and fluorescein protein conjugates by n-propyl gallate. *Science,* **217,** 1252–1255.

Goldstein, D. J., 1980. A microdensitometric method for the analysis of staining kinetics. *J. Microsc.*, **119,** 331–343.

Gonzalez, R. C. and Woods, R. E., 1993. *Digital Image Processing*, pp. 221–225. Addison-Wesley, Reading, Mass.

Gray, P., 1975. *The Microtomist's Formulary and Guide*. Krieger, Huntington, N.Y.

Green, F. J., 1991. *The Sigma–Aldrich Handbook of Stains, Dyes and Indicators*. Milwaukee.

Harms, H., 1965. *Handbuch der Farbstoffe für die Mikroskopie*. Staufen, Kamp-Lintfort.

Haug, H. and Kraus, C., 1958. Vergleichende Untersuchungen über die Celloidin- und Paraffineinbettung. *J. Hirnforsch.*, **4,** 254–271.

Haug, H., 1976. Experiences with optomanual automated evaluation-systems in biological research, especially in neuromorphology. *Proceedings of the 4th International Congress for Stereology*, pp. 167–172.

Heimann, E., 1898. Beiträge zur Kenntnis der feineren Struktur der Spinalganglien. *Virchow. Arch. Path. Anat. Physiol. Klin. Med.*, **152,** 298–336.

Heinsen, H. and Heinsen, Y. L., 1991. Serial thick, frozen, gallocyanin stained sections of human central nervous system. *Journal of Histotechnology,* **14,** 167–173.

Herlin, P., Liu, J.-L., Duigou, F., Marnay, J., Gallet, B., Masson, E., Plancoulaine, B., Bloyet, D. and Mandard, A.-M., 1989. Silver impregnation of biological structures: stainings of potential value for automatic image anaylsis. Proceedings of the European Congress for Stereology 5, *Acta Stereol.* **8,** 523–525.

Hine, B. and Rodriguez, R., 1992. Rapid gelatin embedding procedure for frozen brain tissue sectioning. *Journal of Histotechnology,* **15,** 121–122.

Holmbom, B., Lindström, M., Näslund, U. and Thornell, L.-E., 1991. A method for enzyme- and immunohistochemical staining of large frozen specimens. *Histochemistry,* **95,** 441–447.

Howard, M. J., 1979. A silver carbonate method for cell counts of neurons and glial elements on paraffin embedded brain tissue. *Stain Technology,* **54,** 299–303.

Huerta, M. F., Koslow, S. H. and Leshner, A. I., 1993. The human brain project: an international resource. *TINS,* **16,** 436–438.

Istomin, V. V. and Amunts, K., 1992. Application of mathematical morphology algorithms for automatic quantification of the cytoarchitecture of human neocortex. *Vision Voice Magazine,* **6,** 142–153.

Kiss, R., Larsimont, D. and Huvos, A. G., 1991. Digital cell image-analysis of Ewings-sarcoma. *Anal. Quant. Cytol. Histol.,* **13,** 356–362.

Kiss, R., Gasperin, P., Verhest, A. and Pasteels, J. L., 1992. Modification of the tumor ploidy level by the choice of the tissue taken as diploid reference in digital cell image analysis of Feulgen-stained nuclei. *Modern Pathology,* **5,** 655–660.

Kiss, R., Salmon, I., Camby, I., Gras, S. and Pasteels, J. L., 1993. Characterization of factors in routine laboratory protocols which significantly influence the Feulgen reaction. *Journal of Histochemistry and Cytochemistry,* **41,** 935–945.

Klein-Wisenberg, Av., 1981. Farbmetrik in der Histochemie: Begriffe und Verfahren. *Acta Histochem.*, **Suppl 24,** 267–273.

Korson, R., 1964. A silver stain for deoxyribonucleic acid. *Journal of Histochemistry and Cytochemistry,* **12,** 875–879.

Kriete, A., 1992. *Visualization in Biomedical Microscopies*, pp. 218–220. VCH, Weinheim.

Levine, M. D., 1985. *Vision in Man and Machine*. McGraw-Hill, New York.

Lewis, A., 1991. The confluence of advances in light microscopy: CCD, confocal, near-field and molecular exciton microscopy. In *New Techniques of Optical Microscopy and Microspectroscopy*, ed. R. J. Cherry, pp. 49–89. CRC Press, Boca Raton, Fla.

Lindroos, O. F. C., 1991. Short Nissl staining for incubated cryostat sections of the brain. *Biotech. Histochem.*, **66,** 208–209.

Lyon, H., Schulte, E. and Hoyer, P. E., 1989. The correlation between uptake of methyl green and Feulgen staining intensity of cell nuclei. An image analysis study. *Histochemistry Journal,* **21,** 508–513.

Mason, W. T., Hoyland, J., Davison, I., Carew, M. A., Jonassen, J., Zorec, R., Lledo, P. M., Shankar, G. and Horton, M., 1993. Technology for real time fluorescent ratio imaging in living cells using fluorescent probes for ions. In *Molecular Imaging in Neuroscience*, ed. N. A. Sharif, pp. 171–207. Oxford University Press, Oxford.

Müller, T., 1994. Large nerve cells with long axons in the granular layer and white matter of the murine cerebellum. *Journal of Anatomy,* **184,** 419–423.

Munasinghe, J. P., Gresham, G. A., Carpenter, T. A. and Hall, L. D., 1995. Magnetic resonance imaging of the normal mouse brain: comparison with histologic sections. *Lab. Anim. Sci.,* **45,** 674–679.

Oud, P. S., Zahniser, D. J., Vooijs, G. P., Raaymakers, M. C. T. and van de Walle, R. T., 1981. Thionine-Feulgen congo red—a new staining technique for automated cytology. *Acta Histochem.*, **Suppl 24,** 199–206.

Perry, S. F., 1981. Improved method for demonstration of cut surfaces of tissue in paraffin blocks. *Mikroskopie,* **38,** 13–15.

Piller, H., 1977. *Microscope Photometry*. Springer, Berlin.

Powers, M. M., 1960. Darrow red, a new basic dye. *Stain Technology,* **35,** 19–21.

Pratt, W. K., 1978. *Digital Image Processing*, pp 50–90. Wiley, New York.

Proescher, F. and Arkush, A. S., 1928. Metallic lakes of the oxazines as nuclear stain substitutes for hematoxylin. *Stain Technology,* **3,** 28–38.

Rális, H. M., Beesley, R. A. and Rális, Z. A., 1973. *Techniques in Neurohistology*. Butterworths, London.

Ramm, P. and Kulick, J. H., 1985. Principles of computer-assisted imaging in autoradiographic densitometry. In *The Microcomputer in Cell and Neurobiology Research*, ed. R. R. Mize, pp. 311–334. Elsevier, New York.

Reusche, E., 1991. Silver staining of senile plaques and neurofibrillary tangles in paraffin sections. *Path. Res. Preact.*, **187,** 1045–1049.

Romeis, B. (1989) *Mikroskopische Technik*. Urban & Schwarzenberg, München.

Rosene, D. L., Roy, N. J. and Davis, B. J., 1986. A cryoprotection method that facilitates cutting frozen sections of whole monkey brains for histological and histochemical processing without freezing artifact. *Journal of Histochemistry and Cytochemistry,* **34,** 1301–1315.

Rüter, A., Harms, H. and Aus, H. M., 1978. Digitale Auswertung der Farbinformation von lichtmikroskopischen Zellbildern. *Informatik-Fachberichte,* **17,** 310–317.

Rüter, A., Harms, H. and Aus, H. M., 1979. Die genormte Farbmessung mit dem Lichtmikroskop als Erweiterung der zytophotometrischen Methodik. In *Angewandte Szenenanalyse*, ed. J. P. Foith, pp. 294–302. Springer, Berlin.

Rüter, A., Wittekind, D., Harms, H. and Aus, H.M., 1980. Genormte Farbmessung und automatische Zytophotometrie in Azur B-Eosin gefärbten Präparaten. In *Erzeugung und Analyse von Bildern und Strukturen*, eds S. J. Pöppl and H. Platzer, pp. 133–145. Springer, Berlin.

Russ, J. C., 1991. *Computer Assisted Microscopy*, pp. 117–119. Plenum Press, New York.

Salmon, I., Camby, I., Gras, T., Rombuat, K., Pasteels, J.-L. and Kiss, R., 1994. The use of digital cell image-analysis of Feulgen-stained nuclei to quantitatively describe morphonuclear features in a series of 174 meningiomas. *Mod. Pathol.*, **7,** 570–577.

Sauer, B., 1980. Eine quantitative automatische Methode zur Untersuchung von menschlicher Hirnrinde am Beispiel der Area striata normaler, adulter Gehirne. Medical dissertation, Hannover, Germany.

Sauer, B., 1983. Semi-automatic analysis of microscopic images of the human cerebral cortex using the gray level index. *J. Microsc.*, **129,** 75–87.

Sauer, B., 1983. Quantitative analysis of the laminae of the striate area in man. An application of automatic image analysis. *J. Hirnforsch.*, **24,** 89–97.

Sauer, B., 1983. Lamina boundaries of the human striate area compared with automatically-obtained gray level index profiles. *J. Hirnforsch.*, **24,** 79–87.

Sauer, B., Dietl, H. W., Kretschmann, H.-J. and Mehraein, P., 1986. A quantitative study of the cerebral cortex in Alzheimer's disease and senile dementia using an automatic image analyzing system. *J. Hirnforsch.*, **27,** 695–702.

Schleicher, A., Zilles, K. and Kretschmann, H.-J., 1978. Automatische Registrierung und Auswertung eines Grauwertindex in histologischen Schnitten. *Verh. Anat. Ges.*, **72,** 413–415.

Schleicher, A., Zilles, K., 1983. Der Einsatz automatischer Fernsehbildanalysatoren, Grenzen und Möglichkeiten. *Verh. Anat. Ges.*, **77,** 189–199.

Schleicher, A., Zilles, K. and Wree, A., 1986. A quantitative approach to cytoarchitectonics: software and hardware aspects of a system for the evaluation and analysis of structural inhomogeneities in nervous tissue. *J. Neurosci. Meth.*, **18,** 221–235.

Schleicher, A., 1990. A quantitative approach to cytoarchitectonics: analysis of structural inhomogeneities in nervous tissue using an image analyser. *J. Microsc.*, **157,** 367–381.

Schmidt, U. and Merck, E., 1993. Microscopic stains. In *Ullmann's Encyclopedia of Industrial Chemistry*, Vol. A24, pp. 567–580.

Schmitt, O., Eggers, R. and Haug, H., 1995a. Quantitative investigations into the histostructural nature of the human putamen. I. Staining, cell classification and morphometry. *Ann. Anat.*, **177,** 243–250.

Schmitt, O., Eggers, R. and Haug, H., 1995b. Quantitative investigations into the histostructural nature of the human putamen. II. The differentiated topological distribution of certain neuron type arrangements. *Ann. Anat.*, **177,** 455–465.

Schmitt, O., 1995c. unpublished data.

Segarra, J. M., 1970. Histological and histochemical staining methods: A selection. In *Neuropathology. Methods and Diagnosis*, eds C. G. Tedeschi and J. M. Foley, pp. 233–269. Little, Brown, Boston.

Sonka, M., Hlavac, V. and Boyle, R., 1993. *Image Processing, Analysis and Machine Vision*, pp. 15–19. Chapman & Hall, Cambridge.

Spacek, J., 1992. Dynamics of Golgi impregnation in neurons. *Microsc. Res. Techn.*, **23,** 264–274.

Supprian, T., Senitz, D. and Beckmann, H., 1993. Presentation of human neocortical neurons stained with the carbocyanine dye DiI compared to the Golgi silver impregnation technique. *J. Hirnforsch.*, **34,** 403–406.

Talve, L. A. I., Collan, Y. U. I. and Alanen, K. A., 1995. Bleaching of melanin before image cytometry of the DNA content of pigmented skin tumors. *Anal. Quant. Cytol. Histol.*, **17,** 344–350.

Taylor, J., Puls, J., Sychra, J. J., Bartels, P. H., Bibbo, N. and Wied, G. L., 1978. A system for scanning biological cells in three colors. *Acta Cytol.*, **22,** 29–35.

Thiessen, G. and Thiessen, H., 1977. Microspectrophotometric cell analysis. *Prog. Histochem. Cytochem.*, **9,** 1–156.

Toga, A. W. and Arnica-Sulze, T. L., 1987. Digital image reconstruction for the study of brain structure and function. *J. Neurosci. Meth.*, **20,** 7–21.

Toga, A. W., 1990. *Three-Dimensional Neuroimaging*. Raven Press, New York.

Toga, A. W. and Banerjee, P. K., 1993. Registration revisited. *J. Neurosci. Meth.*, **48,** 1–13.

Toga, A. W., Ambach, K., Quinn, B., Hutchin, M. and Burton, J. S., 1994. Postmortem anatomy from cryosectioned whole human brain. *J. Neurosci. Meth.*, **54,** 239–252.

Toga, A. W., 1995. A 3D digital map of rat brain. *Brain Research Bulletin*, **38,** 77–85.

Tolivia, J., Navarro, A. and Tolivia, D., 1994. Differential staining of nerve cells and fibres for sections of paraffin-embedded material in mammalian central nervous system. *Histochemistry*, **102,** 101–104.

Vacca, L. L., 1985. *Laboratory Manual of Histochemistry*. Raven Press, New York.

Wenzelides, K., 1982. Zur Darstellung der Leberzellgrenzen mit Anilinblau und ihre automatische Erfassung mit einem Bildanalysesystem. *Acta Histochem.*, **70,** 193–199.

Wittekind, D., 1981. Biologische Farbstoffe: Definition, Zugehörigkeit zu Chemie und Morphologie; Farbstoffe als Werkzeuge der Histochemie. *Acta Histochem.*, **Suppl 24,** 133–150.

Wölker, W., 1993. Ein Verfahren zur Farbraumanpassung CCD-basierter Bilderfassungssysteme. In *Informatik aktuell*. Mustererkennung 1993, eds S. J. Pöppl and H. Handels, pp. 749–756. Springer, Berlin.

Wree, A., Schleicher, A., Zilles, K., 1982. Estimation of volume fractions in nervous tissue with an image analyzer. *J. Neurosci. Meth.*, **6,** 29–43.

Wree, A., Zilles, K., Schleicher, A. and Schwientek, P., 1983. Quantitative Cytoarchitektonik des primären visuellen Cortex der Ratte. *Verh. Anat. Ges.*, **77,** 249–250.

Wree, A., Zilles, K. and Schleicher, A., 1983. A quantitative approach to cytoarchitectonics. VIII. The areal pattern of the cortex of the albino mouse. *Anat. Embryol.*, **166,** 333–353.

Yemma, J. J. and Penza, S. L., 1987. Effects of chemistry, manufacturing and concentration of the dye basic fuchsin regarding its use in quantitative cytophotometry. *Cytobios.*, **50,** 13–28.

Zandona, C., Budel, V., Larsimont, D., Petein, M., Gasperin, P., Pasteels, J-L. and Kiss, R., 1994. Digital cell image-analysis of Feulgen-stained nuclei from human papillary, medullary, colloid, lobular and comedocarcinomas of the breast. *Anticancer Research*, **14,** 2173–2182.

Zilles, K., 1978. A quantitative approach to cytoarchitectonics. I. The areal pattern of the cortex of Tupaia belangeri. *Anat. Embryol.*, **153,** 195–212.

Zilles, K., 1978. Automatic morphometric analysis of retrograde changes in the nucleus n. facialis at different ontogenetic stages in the rat. *Cell Tissue Research*, **190,** 285–299.

Zilles, K., Rehkämper, G. and Schleicher, A., 1979. A quantitative approach to cytoarchitectonics. V. The areal pattern of the cortex of *Microcebus murinus* (E. Geoffroy 1828), (Lemuridae Primates). *Anat. Embryol.*, **157,** 269–289.

Zilles, K., Rehkämper, G., Stephan, H. and Schleicher, A., 1979. A quantitative approach to cytoarchitectonics. IV. The areal pattern of the cortex of *Galago demidovii*. *Anat. Embryol.*, **157,** 81–103.

Zilles, K., Zilles, B. and Schleicher, A., 1980. A quantitative approach to cytoarchitectonics. VI. The areal pattern of the cortex of the albino rat. *Anat. Embryol.*, **159,** 335–360.

Zilles, K., 1981. The telencephalon of *Ichthyophis paucisulus* (Amphibia, Gymnophonia (=Caecilia)). A quantitative cytoarchitectonic study . *Z. Mikrosk.-Anat. Forsch.*, **95,** 943–962.

Zilles, K., Blohm, U. and Koch, I., 1983. Neurohistologische Methoden. 1. *Markscheidenfärbung, Mta Praxis*. **29,** 205–207.

Zilles, K., Wree, A., Schleicher, A. and Divac, I., 1984. The monocular and biocular subfields of the rat's primary visual cortex: a quantitative morphological approach. *J. Comp. Neurol.*, **226,** 391–402.

Zilles, K., Armstrong, E., Schlaug, G. and Schleicher, A., 1986. Quantitative cytoarchitectonics of the posterior cingulate cortex in primates. *J. Comp. Neurol.*, **253,** 514–524.